

Anomalous Mean-Squared Displacement in Quantum Active Matter from a Wigner Phase-Space Framework

Sangyun Lee,^{1,*} Yehor Tuchkov,¹ Alexander P. Antonov,² Benno Liebchen,³ Hartmut Löwen,² Giovanna Morigi,⁴ and Michael te Vrugt^{1,†}

¹*Institut für Physik, Johannes Gutenberg-Universität Mainz, 55128 Mainz, Germany*

²*Institut für Theoretische Physik II: Weiche Materie, Heinrich-Heine-Universität Düsseldorf, Universitätsstraße 1, D-40225 Düsseldorf, Germany*

³*Institut für Physik der kondensierten Materie, Technische Universität Darmstadt, Hochschulstraße 8, D-64289 Darmstadt, Germany*

⁴*Theoretische Physik, Universität des Saarlandes, Campus E26, D-66123 Saarbrücken, Germany*

(Dated: April 27, 2026)

Active matter is driven out of equilibrium by a local influx of energy. While classical active matter has been extensively studied, the extension of active matter concepts to quantum systems has been explored far less. In this work we develop a full quantum description based on the Wigner function. By introducing a hybrid Wigner master equation that incorporates classical active motion and quantum degrees of freedom, we compute the quantum mean-squared displacement (MSD) using established techniques from classical active matter. We analytically derive the time dependence of the MSD and clarify the conditions under which the characteristic scaling with time $\text{MSD} \sim t^6$ emerges. We further show that, for certain parameter and initial conditions, the MSD can exhibit an even steeper scaling regime $\text{MSD} \sim t^7$, and we examine the robustness of these behaviors against quantum fluctuations of the initial state.

I. INTRODUCTION

Active matter [1–3] refers to nonequilibrium systems consisting of units that continuously convert internal or environmental energy into directed motion. Across micro- and macroscales, these systems display a wide range of nonequilibrium phenomena, from ballistic motion at the single-particle level [4] to spontaneous self-organization at the collective level [5–8]. Typical examples of active matter include living organisms [9, 10] and robots [11–13] on the macroscale and bacteria [14] or Janus particles [15, 16] on the microscale. Although the smallest active objects, such as enzymes [17, 18], can be as small as several nanometers, this is still far beyond the scale where the quantum effects typically emerge. However, recent advances in the control of individual atoms in the quantum regime have made the experimental realization of active particle exhibiting quantum behavior conceivable, raising the fundamental question for how to define quantum active matter [19].

Quantum active matter refers to active matter whose behavior is affected by quantum effects such as interference, entanglement, quantum statistics and discretization of energy levels. It is an emerging research area and, so far, only a few studies have addressed quantum active matter [20–26]. One approach [21] is to model quantum active matter using spin systems. In particular, a lattice model of hard-core bosons with spin-dependent asymmetric hopping, which acts as an activity, has been shown to exhibit activity-induced ferromagnetism. Waveguide systems have been proposed as a platform for implementing quantum active matter and realizing nonreciprocal phase transitions [24]. Another approach [22] combines a quantum system with a classical active system, allowing the quantum system to inherit activity from the classical dynamics. In this setup, the Heisenberg uncertainty principle forbids a simultaneous sharply localized initial distribution in both position and momentum. Within this framework, the MSD of quantum active matter, which is one of the key physical quantities characterizing activeness, was investigated, and an unusual t^6 scaling of the MSD was reported in Ref. [22]. This scaling is anomalous in the context of active matter, where the MSD of systems such as run-and-tumble particles and the active Ornstein–Uhlenbeck process typically exhibits a ballistic t^2 regime at short times and crosses over to diffusive scaling, $\sim t$, at long times.

In quantum systems, a single point in phase space does not correspond to a realizable event in the classical probabilistic sense, due to the noncommutativity of quantum observables. Nevertheless, phase-space representations such as Wigner transformation [27, 28] remain useful, particularly for extending classical systems to the quantum regime, where intuition from classical dynamics plays a central role [29]. Furthermore, in some systems, this representation even allows the use of classical analytical or computational tools to analyze quantum dynamics. Therefore, in the

* sanlee@uni-mainz.de

† tevrugtm@uni-mainz.de

context of quantum active matter, which combines intrinsically nonequilibrium driving with quantum fluctuations, such a representation can be valuable.

In this paper, we further investigate the condition and robustness of the anomalous t^6 scaling reported for the MSD of a system which mimicking quantum active matter [22]. The numerical analysis revealing the t^6 scaling in Ref. [22] was based on the long-time-limit expression for the quantum MSD and a quantum master equation valid in small activity regime. Here we extend this analysis by evaluating the MSD without the long-time approximation and by considering an open quantum master equation valid beyond small activity regime [23]. In addition, we choose the initial condition such that the activity contributes already at $t = 0$, allowing us to capture the influence of activity from the earliest stage of the dynamics.

To this end, we employ a hybrid Wigner master equation to analytically evaluate the MSD of the quantum active matter. Compared to the previous studies [22, 23], our framework enables the derivation of an exact analytical expression for the MSD, allowing us to systematically characterize its scaling behavior and identify the regimes in which the t^6 scaling emerges. We systematically characterize the behavior of the MSD and find the regime where the t^6 scaling emerges. In addition to finding the emergence condition of the t^6 scaling, we find that for the initial condition that is considered in earlier work [23] the MSD can also exhibit a t^7 scaling regime in the limit of strong active diffusion. Finally, we examine the robustness of these anomalous scalings with respect to the choice of the initial quantum state.

II. WIGNER TRANSFORMATION

Let us first outline the general idea of this paper: To investigate the behavior of the MSD, we introduce a hybrid Wigner master equation that handles classical and quantum randomness on a phase space. As the hybrid Wigner master equation has the same mathematical structure as the classical Fokker-Planck equation, the hybrid master equation allows us to employ established tools from classical active matter, for example to calculate the MSD of the underlying quantum system. This provides an efficient way to analyze the quantum active matter.

We start by introducing the ordinary Wigner transformation [27]. In quantum systems, due to the uncertainty principle, certain pairs of physical observables cannot be measured simultaneously. Such pairs are characterized by non-commuting operators. For example, position and momentum cannot be measured simultaneously. As a consequence, the probability distribution of states in phase space does not exist in quantum physics. The Wigner transformation provides a useful tool that nevertheless allows a quantum system to be represented in phase space in a manner analogous to that of a classical system. This representation enables a comparison between classical and quantum dynamics [30, 31], and also offers insights into quantum extensions of classical theories, as early works on open quantum systems [29]. The Wigner function is not a probability distribution, since individual points in phase space do not correspond to realizable physical events. In other words, it cannot be interpreted as a joint probability distribution because position and momentum cannot be simultaneously measured in a physical experiment. Moreover, the value of Wigner function can be negative, in particular for non-Gaussian quantum state [32].

The Wigner transformation [33] is defined as follows: For an operator \hat{A} , the Wigner transform of an operator \hat{A} is given by

$$A_W(x, p) \equiv \Xi[\hat{A}] = \frac{2}{\hbar} \int dz e^{-\frac{2ipz}{\hbar}} \langle x + z | \hat{A} | x - z \rangle. \quad (1)$$

Here \hbar is the reduced Planck's constant and $\hat{\cdot}$ denotes quantum operator. Here, x and p represent the phase-space variables of the quantum system. For classical systems, a subscript c is used to distinguish their state variables from those of the quantum phase space. For the density matrix $\hat{\rho}$, the corresponding Wigner function reads

$$W(x, p, t) \equiv \frac{1}{2\pi} \Xi[\hat{\rho}(t)] \quad (2)$$

where the factor $1/(2\pi)$ is required for normalization.

The dynamics of an open quantum system, such as the Lindblad master equation, can also be described in terms of the Wigner function and the Moyal product. Assuming an open quantum master equation with system Hamiltonian \hat{H} and a dissipator $\mathcal{D}_{\text{diss}}$, the master equation is written as

$$\frac{d\hat{\rho}(t)}{dt} = -\frac{i}{\hbar} [\hat{H}, \hat{\rho}(t)] + \mathcal{D}_{\text{diss}}[\hat{\rho}(t)], \quad (3)$$

In our work, we consider a Lindblad dissipator [27] for $\mathcal{D}_{\text{diss}}$. After the Wigner transformation [27, 28, 34], Eq. (3) is given by

$$\partial_t W(x, p) = H_W \star W - W \star H_W + D_{\text{diss}}[W] \quad (4)$$

$$\equiv \mathcal{L}_W W(x, p) \quad (5)$$

where $H_W = \Xi[\hat{H}]$ is the Wigner transformed Hamiltonian in and \star denotes the Moyal product (See Appendix. A for more information on Moyal product.)

$$(f \star g)(x, p) \equiv f(x, p) \exp\left[\frac{i\hbar}{2} \left(\overleftarrow{\partial}_x \overrightarrow{\partial}_p - \overleftarrow{\partial}_p \overrightarrow{\partial}_x\right)\right] g(x, p). \quad (6)$$

Here, $\overleftarrow{\partial}_y$ ($\overrightarrow{\partial}_y$) denotes the derivative operator acting on the function to its left (right), respectively. In Eq. (4), $H_W \star W - W \star H_W$ describes the evolution generated by the Liouville operator $-i\hbar[\hat{H}, \hat{\rho}]$ and $D_{\text{diss}}[W]$ denotes dissipation by external environment. Using computer algebra software such as *Mathematica* [35], the transformation can be carried out easily. We provide our code that can handle the Wigner transformation analytically in Ref. [36]. Also, in Appendix. C, we provide detailed information on our code. The operator expectation values can be calculated in terms of the phase-space averaging with W . For example, the expectation of a symmetrized one-time operator is equivalent to the expectation value of the corresponding one-time function in the Wigner phase space (see appendix B). Therefore, Eq. (4) can be utilized to calculate physical quantities.

We can interpret Eq. (5) as a classical Fokker–Planck equation, when the Wigner master equation is quadratic in ∂_x and ∂_p and the initial condition is a Gaussian function. The mentioned condition ensures that the Wigner function is always positive. Therefore, there exists the corresponding Langevin equation to the Wigner master equation, in the same way that a stochastic process governed by a Langevin equation can be equivalently described by a classical Fokker–Planck equation. This is referred to as a quasiclassical Langevin equation [28]. Even when the Wigner function becomes negative in certain regions of phase space and the quantum master equation is quadratic to \hat{x} and \hat{p} , the time evolution of its moments coincides with that obtained from the corresponding classical Fokker–Planck equation and from the associated Langevin equations [28].

For example, let us assume that Wigner master equation is quadratic in ∂_x and ∂_p and that its drift vector and diffusion matrix are given by a linear function $\mathbf{f}(\mathbf{q}, t)$ and BB^T , respectively. Then, the master equation introduced above corresponds to the quasiclassical Langevin equation

$$\dot{\mathbf{q}}(t) = \mathbf{f}(\mathbf{q}, t) + B \cdot \boldsymbol{\eta}(t) \quad (7)$$

where $\langle \eta_i(t) \eta_j(t') \rangle = 2\delta_{ij} \delta(t - t')$. Note that \mathbf{q} is a real-valued vector representing coordinates in Wigner phase space and does not correspond to an operator. The vector \mathbf{f} is a linear function of \mathbf{q} . Because nonlinear force terms lead to higher-order derivatives $\partial_{\mathbf{q}}^n$ ($n > 2$) in the Wigner master equation, they cannot be handled by such a quasiclassical Langevin equation.

In this work, we focus on a heat bath described by a Lindblad master equation [23] and determine the MSD scaling with time. Since the t^6 scaling [22] was identified in the non-dissipative regime $\mathcal{D}_{\text{diss}}[\hat{\rho}(t)]$, the specific choice of quantum heat bath does not affect the conditions for the emergence of the t^6 or t^7 scalings that we will discuss. The Lindblad master equation with a harmonic potential centered at $x = x_c$, given by $\hat{U}(x) = m\omega^2(\hat{x} - x_c)^2/2$, where m is the mass of the system and ω is the frequency of the trap leads to the quasiclassical Langevin equation [23, 30, 31]

$$\partial_t x = \frac{p}{m} - \gamma(x - x_c) + B_x \eta_x(t), \quad (8a)$$

$$\partial_t p = -m\omega^2(x - x_c) - \gamma p + B_p \eta_p(t), \quad (8b)$$

where γ and B_i are friction and diffusion coefficients. The thermostat acting on the positional degrees of freedom contributes to the initial linear behavior of the quantum MSD. We will explain this point in the following section. The inhomogeneous damping in Eq. (8a) is unavoidable when one employs a Markovian master equation with a harmonic oscillator satisfying complete positivity and trace preservation (CPTP) [37].

Various types of quantum active matter can be modeled using a different quantum bath [23]. For reference, we also present here the Caldeira–Leggett form [27], although it is not used in the present work. The corresponding quasiclassical Langevin equation for a harmonic oscillator has the following mathematical structure [28, 30]

$$\partial_t x = \frac{p}{m} \quad (9a)$$

$$\partial_t p = -m\omega^2(x - x_c) - \gamma p + B_p \eta_p(t). \quad (9b)$$

One can see that the mathematical structure is the same as the one from ordinary classical systems. However, the map generated by the Caldeira-Leggett master equation does not satisfy the CPTP condition. For further details about quantum active matter using this type of bath, see Ref. [27].

For the above quasiclassical Langevin equations, one finds that they belong to the class of Ornstein—Uhlenbeck processes. This allows us to employ established techniques commonly used in classical active matter physics to analyze the dynamics of the quantum system. In the following, we show how the MSD can be calculated analytically using methods developed for classical systems.

Due to the correspondence of one-time correlation function, the quasiclassical Langevin equation can be utilized to calculate quantum expectation values. The MSD is an important quantity that characterizes a system in a wide range of systems from active matter to glassy systems [38]. In the Heisenberg picture, it is defined by

$$\langle [\hat{x}(t) - \hat{x}(0)]^2 \rangle_{\hat{\rho}} = \langle \hat{x}(t)^2 \rangle_{\hat{\rho}} - \langle \hat{x}(t)\hat{x}(0) \rangle_{\hat{\rho}} - \langle \hat{x}(0)\hat{x}(t) \rangle_{\hat{\rho}} + \langle \hat{x}(0)^2 \rangle_{\hat{\rho}} \quad (10)$$

where $\langle \cdot \rangle_{\hat{\rho}}$ denotes average over a density matrix, $\hat{\rho}$. Although we assume here a one-dimensional system, this definition straightforwardly extends to an N -dimensional system. We note that the definition of the MSD used in this work [Eq. (10)] differs from that employed in Refs. [22, 23], where the MSD is defined without involving two-time correlation functions.

The MSD contains a symmetrized two-time correlation function, which can be calculated from the Wigner master equation or the quasi-classical Langevin equation using the following equality

$$\langle \hat{x}(t)\hat{x}(0) + \hat{x}(0)\hat{x}(t) \rangle_{\hat{\rho}} = \int dx dp [x_W(t) \star x_W(0) + x_W(0) \star x_W(t)] W(x, p, 0). \quad (11)$$

Here, taking $\hat{A} = \hat{x}, \hat{p}$ in Eq. (1), the corresponding Wigner functional is $x_W(t)$ and $p_W(t)$. Under the sufficient condition that $\hat{x}(t)$ can be expressed as a linear function of $\hat{x}(0)$ and $\hat{p}(0)$, the right hand-side of Eq. (11) reduces to a simpler form, and the two-time correlation functions calculated in terms of the Wigner function are equal to the operator expectation of the symmetrized two-time correlation function.

$$\langle \hat{x}(t)\hat{x}(0) + \hat{x}(0)\hat{x}(t) \rangle_{\hat{\rho}} = 2 \int dx dp x_W(t)x_W(0)W(x, p, 0) \quad (12)$$

In Appendix B, we present a general proof of the equivalence, from which Eq. (12) follows as a special case. Equation (12) provides a convenient form for calculations, and, in the remainder of this paper, we focus on systems for which this equality holds.

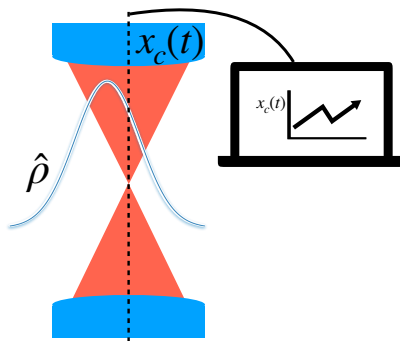


FIG. 1. Conceptual figure to illustrate the quantum active matter model from Ref. [23]. The Hamiltonian for this system is given by Eq. (18). The optical tweezers exert harmonic force on the quantum system, $\hat{\rho}$. The computer generates activity term $x_c(t)$, and the center of the optical trap follows the generated trajectory $\Gamma_c = \{x_c(t)\}$.

III. HYBRID WIGNER MASTER EQUATION

In the context of quantum active matter, one approach [22, 23] to extend classical active matter into the quantum regime is to construct systems that combine classical stochastic dynamics with quantum degrees of freedom. This

scheme is particularly useful for describing systems that mimic quantum active particles. Consider an atom trapped by an optical tweezer whose potential can be approximated as a harmonic oscillator, with its center denoted by $x_c(t)$ (see Fig. 1 for a schematic illustration). The trap center follows a trajectory $\{x_c(t)\}_{0 \leq t}$ generated by numerically solving a classical Langevin equation for active noise. Through the movement of the trap center, the quantum state $\hat{\rho}$ of the atom inherits the features of classical active matter [22, 23].

Since the potential of the quantum active matter follows the classical stochastic equation, it is natural to introduce a hybrid Wigner function that incorporates classical stochasticity alongside quantum dynamics. Let us assume that \mathbf{q}_c is the state of a classical system and $\Gamma_c \equiv \{\mathbf{q}_c(t)\}$ is its trajectory. The distribution of \mathbf{q}_c evolves according to

$$\partial_t P(\mathbf{q}_c, t) = \mathcal{L}_c P(\mathbf{q}_c, t). \quad (13)$$

For a given realization Γ_c , quantum master equation is given by

$$\partial_t W(x, p, t | \Gamma_c) = \mathcal{L}_W W(x, p, t | \Gamma_c) \quad (14)$$

Here, $W(x, p, t | \Gamma_c)$ is attained by Wigner transforming the density matrix ρ_c that is conditioned on a given trajectory \mathbf{q}_c . Then, we define a hybrid quasi-probability distribution which combines the trajectory probability $P[\Gamma_c]$ and the Wigner function

$$W(x, p, \mathbf{q}_c, t) \equiv \int \mathcal{D}[\Gamma_c] W(x, p, t | \Gamma_c) P[\Gamma_c] \delta(\mathbf{q}_c - \mathbf{q}_c(t)). \quad (15)$$

Then, the master equation for the hybrid function is given by

$$\partial_t W(x, p, \mathbf{q}_c, t) = \mathcal{L}_W W(x, p, \mathbf{q}_c, t) + \mathcal{L}_{FP} W(x, p, \mathbf{q}_c, t). \quad (16)$$

In Appendix H, we provide the derivation for the above master equation. Although the derivation in Appendix H assumes specific stochastic differential equation, the result can be straightforwardly extended to a general stochastic differential equation for \mathbf{q}_c .

As there exists an equivalence between the MSD from quantum operative expectation and the one from Wigner space expectation for a given trajectory, the hybrid function also provides the equivalence even after averaging over realization of the classical trajectory $\mathbf{q}_c(t)$. In the following section, we present the application of this equivalence for finding detailed condition for t^6 slope of the MSD of quantum active matter that recently discussed in Ref. [22] and shows the condition when t^7 slope arises.

IV. SCALING INVESTIGATION USING HYBRID WIGNER FUNCTION

We consider the following one-dimensional hybrid quantum master equation describing a quantum system coupled to classical variables for activity x_c and u . This is the model from Ref. [23], expressed in terms of a quantum master equation. It reads

$$\frac{d\hat{\rho}_c(t)}{dt} = -\frac{i}{\hbar} [\hat{H}(x_c(t)), \hat{\rho}_c(t)] + \mathcal{D}[\hat{\rho}_c(t)], \quad (17)$$

where $\Gamma_c = \{x_c(t)\}$ is a given classical trajectory, $\hat{\rho}_c(t) \equiv \hat{\rho}(t; \Gamma_c)$ denotes the density matrix of the quantum system conditioned on the trajectory and $\mathcal{D}[\hat{\rho}_c(t)]$ is the superoperator describing the effects of a thermal heat bath. Here, the commutator is defined as $[\hat{A}, \hat{B}] \equiv \hat{A}\hat{B} - \hat{B}\hat{A}$. This model is designed to describe a moving harmonic potential under the adiabatic approximation; the change rate of the system Hamiltonian is sufficiently slow such that it does not lead to transitions among instantaneous eigenstates [39, 40]. Note that when an observable is averaged over random trajectories, the corresponding probability may be expressed as the combination of the density matrix and the trajectory probability $\hat{\rho}_c(t) P[\{x_c(t)\}]$. For example, in Ref. [22, 23], the averaged over the combined probability was used to evaluate the approximated MSD.

The first term on the right-hand side of Eq. (17) corresponds to the unitary evolution by the Hamiltonian of kinetic energy and harmonic potential centered at x_c :

$$\hat{H}(x_c(t)) = \frac{\hat{p}^2}{2m} + \frac{1}{2} m \omega^2 (\hat{x} - x_c(t))^2. \quad (18)$$

Here, $x_c(t)$ denotes the internal active variable that encodes the active fluctuations. Its dynamics is governed by Ornstein–Uhlenbeck process

$$\dot{x}_c(t) = u(t), \quad (19a)$$

$$\tau \dot{u}(t) = -u(t) + \sqrt{D}\eta(t) \quad (19b)$$

$$= -u(t) + \tau\sqrt{D_u}\eta(t) \quad (19c)$$

where D is a rescaled diffusion coefficient defined in terms of the diffusion coefficient D_u and the persistence time τ as $D \equiv \tau^2 D_u$. η is the Gaussian white noise satisfying $\langle \eta(t)\eta(t') \rangle = 2\delta(t-t')$. In the long-time limit ($t \gg \tau$), D governs the diffusive behavior of x_c , leading to the mean-square displacement,

$$\langle x_c^2(t) \rangle_c \simeq 2Dt. \quad (20)$$

In contrast, D_u is the diffusion coefficient for the auxiliary variable u . In the short-time limit,

$$\langle u^2 \rangle_c \simeq 2D_u t. \quad (21)$$

$\langle \rangle_c$ denotes the average over the noise realizations in Eqs. (19), representing an averaging over classical-thermal fluctuations. The dynamics of the active Ornstein–Uhlenbeck process (AOUP) introduces nonequilibrium fluctuations into the quantum system through $x_c(t)$. $u(t)$ is an auxiliary variable that can be interpreted as the velocity of $x_c(t)$ and allows the dynamics to be expressed as a Markovian process. From now on, we consider the trajectories of x_c and u rather than x_c alone. The second term describes non-unitary evolution and has the Lindblad form

$$\begin{aligned} \mathcal{D}[\hat{\rho}] \equiv & \frac{\gamma}{2} \bar{n} \left(\hat{a}^\dagger(t) \hat{\rho}(t) \hat{a}(t) - \frac{1}{2} \{ \hat{a}(t) \hat{a}^\dagger(t), \hat{\rho}(t) \} \right) \\ & + \frac{\gamma}{2} (\bar{n} + 1) \left(\hat{a}(t) \hat{\rho}(t) \hat{a}^\dagger(t) - \frac{1}{2} \{ \hat{a}^\dagger(t) \hat{a}(t), \hat{\rho}(t) \} \right). \end{aligned} \quad (22)$$

Here, $\bar{n} = [\exp(\hbar\omega/k_B T) - 1]^{-1}$ is the mean number of quanta in equilibrium, and the anti-commutator is defined as $\{ \hat{A}, \hat{B} \} \equiv \hat{A}\hat{B} + \hat{B}\hat{A}$. The creation and annihilation operators $\hat{a}^\dagger(t)$ and $\hat{a}(t)$ are defined with respect to the instantaneous position of the potential minimum $x_c(t)$ as

$$\hat{a}(t) = \sqrt{\frac{m\omega}{2\hbar}} \left(\hat{x} - x_c(t) + \frac{i}{m\omega} \hat{p} \right) \quad (23a)$$

and

$$\hat{a}^\dagger(t) = \sqrt{\frac{m\omega}{2\hbar}} \left(\hat{x} - x_c(t) - \frac{i}{m\omega} \hat{p} \right). \quad (23b)$$

The parameters $\nu_- = \gamma(\bar{n}+1)/2$ and $\nu_+ = \gamma\bar{n}/2$ denote the decay and pumping rates, respectively. ν_- is the prefactor for the term $\hat{a}(t)\hat{\rho}(t)\hat{a}^\dagger(t) - \frac{1}{2}\{\hat{a}^\dagger(t)\hat{a}(t), \hat{\rho}(t)\}$ in Eq. (22), which reduces the number of quanta in the system. ν_+ is the prefactor for the term $\hat{a}^\dagger(t)\hat{\rho}(t)\hat{a}(t) - \frac{1}{2}\{\hat{a}(t)\hat{a}^\dagger(t), \hat{\rho}(t)\}$ in Eq. (22), which increases the number of quanta in the system.

We now introduce the Wigner representation of the hybrid quantum–classical system. The Wigner transform of the density matrix of a given trajectory of $x_c(t)$ and $u(t)$ is defined as

$$W_c(x, p, t) \equiv \mathcal{W}[\hat{\rho}_c(t)|\Gamma_c]. \quad (24)$$

Here, the trajectory is written as $\Gamma_c = \{x_c(t), u(t)\}$. For a given $\{x_c(t)\}$, the Wigner equation is given by

$$\begin{aligned} \partial_t W_c(x, p, t) &= \partial_i [f_i W_c(x, p, t)] + \partial_{ij}^2 [g_{ij} W_c(x, p, t)], \\ &\equiv \mathcal{L}_W W_c(x, p, t), \end{aligned} \quad (25)$$

where the drift vector and the diffusion matrix are given by

$$f_i = \left(-\frac{p}{m} + \frac{\gamma}{4}(x - x_c), \right. \\ \left. m\omega(x - x_c) + \frac{\gamma}{4}p \right), \quad (26a)$$

and

$$g_{ij} = \begin{pmatrix} \frac{\gamma\hbar}{8m\omega} \coth\left(\frac{\hbar\omega}{2k_B T}\right) & 0 \\ 0 & \frac{\gamma\hbar m\omega}{8} \coth\left(\frac{\hbar\omega}{2k_B T}\right) \end{pmatrix}. \quad (26b)$$

For the derivation of Eq. (25) see Ref. [23]. Here, we introduce the hybrid Wigner function such that

$$W(x, p, x_c, u, t) = \int \mathcal{D}[\Gamma_c] W_c(x, p, t) P[\Gamma_c] \delta(x_c - x_c(t)) \delta(u - u(t)). \quad (27)$$

Then, by following a derivation analogous to that of the differential Chapman–Kolmogorov equation [41, 42], the master equation for the hybrid Wigner function is written by

$$\partial_t W(x, p, x_c, u, t) = \mathcal{L}_w W(x, p, x_c, u, t) + \mathcal{L}_{\text{FP}} W(x, p, x_c, u, t) \quad (28)$$

where \mathcal{L}_{FP} is the generator for the evolution of the AOUP. In Appendix. H, we present the detailed derivation. The Fokker–Planck equation for the AOUP [Eqs. (19)] reads

$$\begin{aligned} \partial_t P(x_c, u, t) &= (\partial_{x_c}, \partial_u) \cdot \begin{pmatrix} 0 & -1 \\ 0 & \frac{1}{\tau} \end{pmatrix} \cdot \begin{pmatrix} x_c \\ u \end{pmatrix} P(x_c, u, t) \\ &+ (\partial_{x_c}, \partial_u) \cdot \begin{pmatrix} 0 & 0 \\ 0 & D_u \end{pmatrix} \cdot \begin{pmatrix} \partial_{x_c} \\ \partial_u \end{pmatrix} P(x_c, u, t) \end{aligned} \quad (29)$$

$$\equiv \mathcal{L}_{\text{FP}} P(x_c, u, t), \quad (30)$$

which is straightforwardly derived from the classical Langevin equation, Eq. 19.

Therefore, the master equation for the hybrid Wigner function is given by this hybrid Fokker–Planck equation

$$\begin{aligned} \partial_t W(x, p, x_c, u, t) &= (\partial_x, \partial_p, \partial_{x_c}, \partial_u) \cdot \begin{pmatrix} \frac{\gamma}{4} & -\frac{1}{m} & -\frac{\gamma}{4} & 0 \\ m\omega^2 & \frac{\gamma}{4} & -m\omega^2 & 0 \\ 0 & 0 & 0 & -1 \\ 0 & 0 & 0 & \frac{1}{\tau} \end{pmatrix} \cdot \begin{pmatrix} x \\ p \\ x_c \\ u \end{pmatrix} W(x, p, x_c, u, t) \\ &+ (\partial_x, \partial_p, \partial_{x_c}, \partial_u) \cdot \begin{pmatrix} \frac{\gamma\hbar}{8m\omega} \coth\left(\frac{\hbar\omega}{2k_B T}\right) & 0 & 0 & 0 \\ 0 & \frac{\gamma\hbar m\omega}{8} \coth\left(\frac{\hbar\omega}{2k_B T}\right) & 0 & 0 \\ 0 & 0 & 0 & 0 \\ 0 & 0 & 0 & D_u \end{pmatrix} \cdot \begin{pmatrix} \partial_x \\ \partial_p \\ \partial_{x_c} \\ \partial_u \end{pmatrix} W(x, p, x_c, u, t) \quad (31) \\ &= \mathcal{L}_{\text{hyb}} W(x, p, x_c, u, t). \quad (32) \end{aligned}$$

Since the hybrid Wigner master equation has a Fokker–Planck structure, there can be many corresponding stochastic differential equations [42]. These stochastic differential equations describe the evolution of a classical probability distribution governed by $\partial_t P(x, p, x_c, u, t) = \mathcal{L}_{\text{hyb}} P(x, p, x_c, u, t)$. Because both the hybrid Wigner dynamics and the associated stochastic process are generated by the same operator \mathcal{L}_{hyb} , the time evolution of all moments are equivalent in the two descriptions.

We can write the corresponding quasiclassical Langevin equation as

$$\dot{\mathbf{q}}(t) = -A \cdot \mathbf{q}(t) + B \cdot \boldsymbol{\eta}(t), \quad (33)$$

where

$$A = \begin{pmatrix} \frac{\nu_- - \nu_+}{2} & -\frac{1}{m} & -\frac{\nu_- - \nu_+}{2} & 0 \\ m\omega^2 & \frac{\nu_- - \nu_+}{2} & -m\omega^2 & 0 \\ 0 & 0 & 0 & -1 \\ 0 & 0 & 0 & \frac{1}{\tau} \end{pmatrix}, \quad B = \begin{pmatrix} \sqrt{\frac{\hbar(\nu_+ + \nu_-)}{4m\omega}} & 0 & 0 & 0 \\ 0 & \sqrt{\frac{m\omega\hbar(\nu_+ + \nu_-)}{4}} & 0 & 0 \\ 0 & 0 & 0 & 0 \\ 0 & 0 & 0 & \sqrt{D_u} \end{pmatrix}, \quad \mathbf{q}(t) = \begin{pmatrix} x(t) \\ p(t) \\ x_c(t) \\ u(t) \end{pmatrix}, \quad (34)$$

and

$$\boldsymbol{\eta}(t) = \begin{pmatrix} \eta_x(t) \\ \eta_p(t) \\ 0 \\ \eta_u(t) \end{pmatrix}. \quad (35)$$

Here, η_i is a Gaussian white noise with zero mean and $\langle \eta_i(t) \eta_j(t') \rangle = 2\delta_{ij} \delta(t - t')$. With the Langevin equation, the analytical form for the Mean squared distance can be derived (see Appendix D). The stochastic differential equation

consists of the linear drift term and Gaussian white noise term, which is named Ornstein-Uhlenbeck process [42]. The covariance matrix of $\mathbf{q}(t) - \mathbf{q}(0)$ is given by

$$\begin{aligned} \langle (\mathbf{q}(t) - \mathbf{q}(0)) \otimes (\mathbf{q}(t) - \mathbf{q}(0)) \rangle &= e^{-At} \langle \mathbf{q}(0) \otimes \mathbf{q}(0) \rangle e^{-A^T t} + 2 \int_0^t e^{-A(t-s)} B B^T e^{-A^T (t-s)} ds \\ &\quad - e^{-At} \langle \mathbf{q}(0) \otimes \mathbf{q}(0) \rangle - \langle \mathbf{q}(0) \otimes \mathbf{q}(0) \rangle e^{-A^T t} + \langle \mathbf{q}(0) \otimes \mathbf{q}(0) \rangle. \end{aligned} \quad (36)$$

Then, the mean-squared distance is given by one of the diagonal components of Eq. (36) as

$$\langle |\mathbf{x}(t) - \mathbf{x}(0)|^2 \rangle = [\langle (\mathbf{q}(t) - \mathbf{q}(0)) \otimes (\mathbf{q}(t) - \mathbf{q}(0)) \rangle]_{xx}. \quad (37)$$

Due the aforementioned equivalence, evaluating Eq. (37) provides the MSD of the hybrid system,

$$\int \mathcal{D}[x_c] \langle [\hat{x}(t) - \hat{x}(0)]^2 \rangle_{x_c(t)} = [\langle (\mathbf{q}(t) - \mathbf{q}(0)) \otimes (\mathbf{q}(t) - \mathbf{q}(0)) \rangle]_{xx}, \quad (38)$$

where $\langle \rangle_{x_c(t)}$ denotes the quantum average conditioned on a given trajectory $\{x_c(t)\}$. Note that when numerically evaluating the MSD [Eq. (37)], we solve an ordinary differential equation rather than directly evaluating the integral in Eq. (36). Both approaches are numerically indistinguishable (see Appendix G).

A. MSD with the initial condition $P(x_c, u) = \delta(x_c) \exp\{-u^2/(2D_u\tau)\}/\sqrt{2\pi D_u\tau}$

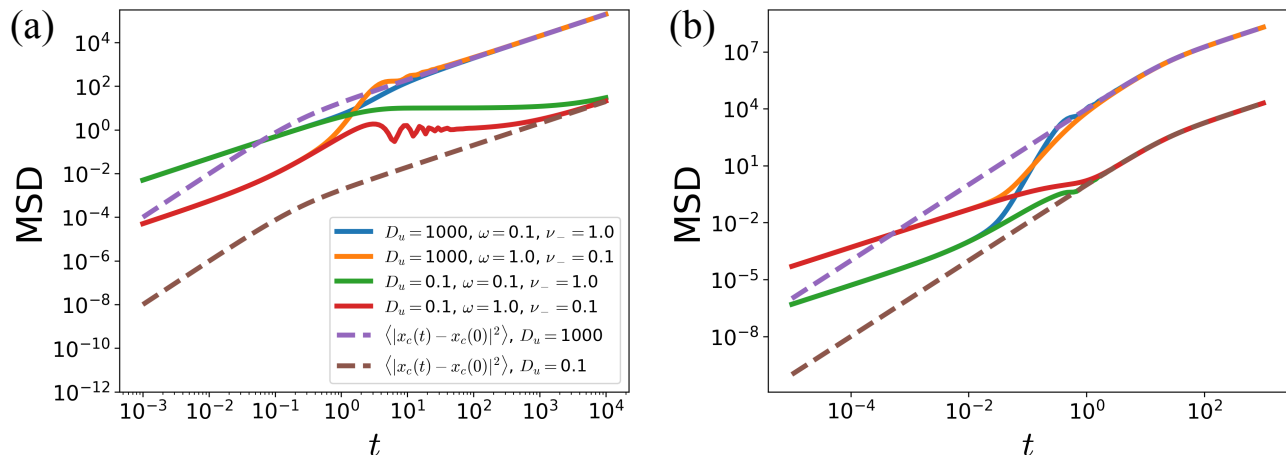


FIG. 2. Plot of MSD versus time of the quantum active particle with the initial conditions, Eq. (39). We varied D_u , ω , ν_- , and ν_+ while fixing the ratio ν_- to ν_+ as 10^4 . Two persistent time were considered: (a) $\tau = 0.1$ case (b) $\tau = 10$ case. The solid lines represent the MSDs with each parameter combinations. The dashed lines represent the MSD of $x_c(t)$. The same color coding is applied to both figures. All quantities in this and the following figures are shown in arbitrary units.

We consider the initial condition of joint distribution of ground state $|0\rangle$ of the harmonic oscillator centered at $x = 0$, while

$$P(x_c, u) = \delta(x_c) \exp\{-u^2/2D_u\tau\}/\sqrt{2\pi D_u\tau}. \quad (39)$$

With this initial condition, the dynamics reduces to that of a classical AOUP with colored noise from the initial time and its MSD is given by

$$\langle |x_c(t) - x_c(0)|^2 \rangle_c = 2D_u\tau^2[t + \tau(-1 + e^{-t/\tau})]. \quad (40)$$

Under this initial condition the MSD of x_c shows scaling transition from t to t^2 . The derivation is same for the Brownian diffusion case (See Section 2 of Ref. [43]). Note that this condition is different from the one in Refs [22, 23]. The latter case will be considered in the following subsection. The system has three characteristic time scales: the

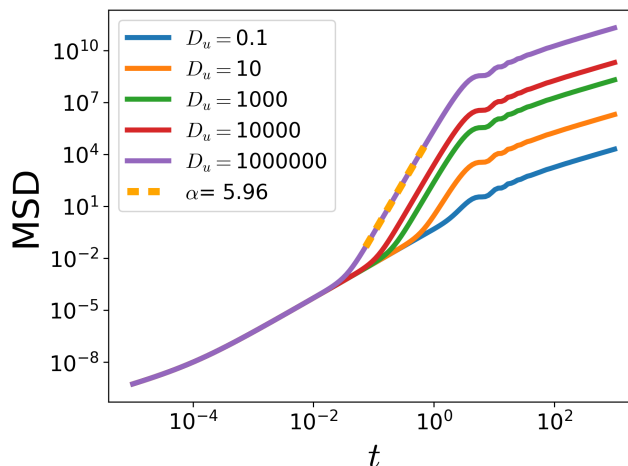


FIG. 3. Plot of MSD versus time of the quantum active particle with different D_u . D_u is varying from 0.1 to 10^6 . Other parameters are chosen as follows: $\omega = 1.0$, $\hbar = 1.0$, $\nu_- = 10^{-4}$, $\nu_+ = 10^{-8}$, and $\tau = 10$. The dashed line represents t^α where $\alpha = 5.9577\dots \pm 0.00296$. We set the mass and Planck constant to unity.

	very early	early	intermediate	late	$t \gg \tau$
Long τ	t		t^α , $\alpha < 6$ or oscillatory	t^2	t
Long τ with weak dissipation	t	t^2	t^α , $\alpha \leq 6$ or oscillatory		
Short τ	t		t^α , $\alpha < 6$	t	
Short τ with weak dissipation	t	t^2	or oscillatory		

TABLE I. MSD of a quantum active particle for different times and parameter regimes.

persistence time τ , the inverse of the harmonic frequency $1/\omega$, and the inverse of the dissipation rate $1/\gamma$. This can be seen in Eq. (36), which implies that the eigenvalues of A govern the time dependence. The eigenvalues of A are given by $\lambda_1 = 0$, $\lambda_2 = 1/\tau$, $\lambda_3 = \gamma/4 - i\omega$ and $\lambda_4 = \gamma/4 + i\omega$. These eigenvalues define the characteristic rates of the dynamics. λ_3 and λ_4 indicate that the MSD oscillates with a high value of ω and a small value of γ .

In Fig. 2, we present two cases (a) $\tau = 0.1$ and (b) $\tau = 10$. In Fig. 2 (a), τ is the shortest time scale among the three characteristic time scales. We consider the two possible orderings $1/\omega > 1/\gamma > \tau$ and $1/\gamma > 1/\omega > \tau$. For each ordering, we examine two values of D_u : a large value ($D_u = 1000$) and a small value ($D_u = 0.1$). In Fig. 2 (b), τ is instead the longest time scale. As in Fig. 2 (a), we consider the same two orderings of time scales, $1/\omega > 1/\gamma > \tau$ and $1/\gamma > 1/\omega > \tau$, again for both $D_u = 1000$ and $D_u = 0.1$.

In both cases, the initial dynamics is primarily governed by ω , whereas the late behavior is determined by the value of D_u . This can be understood from the fact that ω determines the initial variance of position and momentum. The late behavior can be understood the fact that the MSD of the quantum active matter approaches to the MSD of x_c ,

$$\langle |\hat{x}(t) - \hat{x}(0)|^2 \rangle \sim \langle |x_c(t) - x_c(0)|^2 \rangle_c \text{ when } t \rightarrow \infty, \quad (41)$$

and the MSD of x_c transitions from t^2 to t . When τ is the shortest time scale, the MSD converges to that of x_c after the latter enters t scaling. Conversely, when τ is the longest time scale, the MSD of our quantum active matter converges to that of x_c once the latter exhibits ballistic t^2 scaling.

Under the assumption that τ is the longest timescale, we derived the asymptotic form of the MSD

$$\langle |\hat{x}(t) - \hat{x}(0)|^2 \rangle \sim 2D_u\tau^2t + B_0 \left[-g_2(t)e^{-2t/\tau} + g_1(t)e^{-t/\tau} - g_0 \right], \quad (42)$$

where $g_1(t)$ and $g_2(t)$ are linear function of t (see Appendix I for its derivation and explicit forms of coefficients). Therefore, two terms involving exponential decaying factor will be suppressed after $t = \tau$. Eq. (42) implies that after τ the MSD approaches to linear regime as $2D_u\tau^2t$.

In the intermediate regime, various dynamical features appear. If $\gamma = 2(\nu_- - \nu_+)$ is small, the MSD oscillates. When γ is high, the oscillatory behavior vanishes and the scaling of MSD is t^α where $\alpha \leq 6$. Depending on D_u and ω , a decrease of the MSD is also possible, which can be found from Fig. 2 (a). Therefore, in this intermediate regime, a rapid increasing of the MSD can be found.

To further investigate the scaling, we expand Eq. (36) in time t around $t = 0$, focusing on short-time regime. We set ν_- and ν_+ as 0. This leads to

$$\langle |\hat{x}(t) - \hat{x}(0)|^2 \rangle = \frac{\omega}{2m}t^2 - \frac{\omega^3}{24m}t^4 + \left(\frac{D_u\tau\omega^4}{36} + \frac{\omega^5}{720m} \right) t^6 - \frac{D_u\omega^4}{168}t^7 + \mathcal{O}(t^8). \quad (43)$$

Eq. (43) shows that a contribution t^6 exists and suggests that t^6 scaling can be observed with high D_u and τ . Also, positive t^7 scaling is prohibited since the term has a negative sign. Note that setting $\nu_- = 0$ and $\nu_+ = 0$ removes the early linear term $((\nu_- + \nu_+)t\hbar/2m\omega)$ in the above expression. As Eq. (43) is expanded to $t = 0$, Eq. (43) does not explain the MSD at late times.

In Fig. 3, we plot MSDs of the quantum active matter varying D_u . We choose small ν_- and ν_+ to observe a t^6 scaling. As D_u increases, the slope in the intermediate regime approaches to t^6 . For the case $D_u = 10^6$, we performed a fit in the intermediate time regime using the ansatz $d t^\alpha$ where d and α are real values. The resulting exponent is $\alpha = 5.9577\dots \pm 0.00296$, which is very close to 6. For this t^6 scaling, small ν_- and ν_+ (weak dissipation) are necessary. Therefore, the conditions for observing t^6 scaling and the absence of t^7 scaling are verified.

The t^6 scaling was originally predicted in Ref. [22] for the nondissipative case using time-dependent perturbation theory. In that work, the external driving was treated as a perturbation to the quantum harmonic oscillator, $\hat{V}_p(x_c(t)) = m\omega^2\hat{x}_c(t) + m\omega^2x_c^2(t)/2$, so that

$$\hat{H}(x_c(t)) = \frac{\hat{p}^2}{2m} + \frac{1}{2}m\omega^2\hat{x}^2 + \hat{H}_p(x_c(t)). \quad (44)$$

Assuming the perturbation to be small, Antonov *et al.* [22] showed that, at second order in perturbation theory, the leading contribution to the MSD scales as t^6 for small t , while all lower-order terms vanish. In contrast, in the present work we obtain an approximate expression for the MSD by considering the short-time limit. Eq. (43) therefore supports the t^6 scaling from a different perspective, and the explicit coefficients further reveal the conditions under which the t^6 scaling can be observed.

Table I summarizes the scaling behavior of the MSD in different time regimes. We distinguish between long and short persistence times τ , and indicate how the MSD depends on time in the very early, early, intermediate, late, and long-time limit ($t \gg \tau$) regimes. The early time is mainly governed by ω , ν_- and ν_+ . In the weak dissipation case ($\nu_-, \nu_+ \ll 1$), the duration of the linear regime decreases and ballistic behavior can be observed. The intermediate regime are started to be affected by τ and D . In particular, the intermediate regime may exhibit nontrivial power-law scaling, t^α with $\alpha \leq 6$, or oscillatory behavior depending on the dissipation strength. When $1/\gamma < 1/\omega$, oscillatory behavior vanished. High $D_u\tau$ increases α and $\alpha = 6$ can be observed with small ν_- and ν_+ . For long persistence times, the late-time dynamics approaches a ballistic (t^2) regime before crossing over to diffusive (t) scaling, whereas for short τ the crossover structure is modified accordingly.

B. MSD with the initial condition $u(0) = 0$ and t^7 scaling

Now, we consider the same initial condition as in Refs. [22, 23]. The only difference is the distribution of u . Explicitly, this initial condition is the joint distribution of ground state of the harmonic oscillator centered at $x = 0$, while

$$P(x_c, u) = \delta(x_c)\delta(u). \quad (45)$$

This results in the MSD of x_c shows the transient behavior from t^3 scaling at short times to t at long times. Explicitly,

$$\langle |x_c(t) - x_c(0)|^2 \rangle = D_u\tau^2[(-3 - e^{-(2t)/\tau}) + 4e^{-(t/\tau)}]\tau + 2t]. \quad (46)$$

For the derivation, see Appendix J. By Taylor expanding Eq. (46) with respect to time t at $t = 0$, one can check that t^3 is dominant at early times. This t^3 scaling of Eq. (46) implies that the initial condition (45) leads to more rapid scaling of MSD of \hat{x} than t^6 .

We numerically evaluated Eq. (36) with the initial condition (45) and plot the results in Fig. 4. With a long persistence time and a large activity strength D_u , we observe a distinct scaling behavior characterized by a t^7 slope. Specifically, the mean-square displacement initially grows as t^2 around $t \sim 10^0$, crosses over to a t^7 scaling regime near $t \sim 10^1$, and returns to a t^2 growth for $t \gtrsim 10^2$. In the very short-time regime, $t \sim 10^{-4}$, we observe a linear growth of the mean-square displacement induced by diffusivity. By contrast, for relatively smaller activity strength D_u and shorter persistence times, we recover the previously reported t^6 scaling behavior.

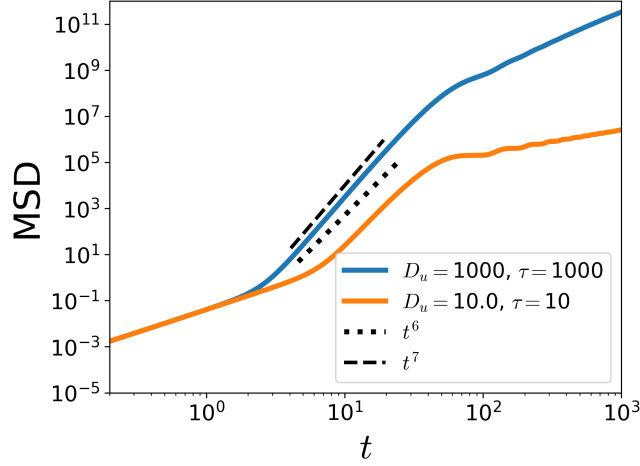


FIG. 4. Plot of MSD versus time of the quantum active particle with different persistent time and noise intensity for the activity. The blue solid line represents the case of long persistent time ($\tau = 1000$) and high intensity ($D_u = 1000$). The orange solid line represents the case of shorter persistent time ($\tau = 10$) and lower intensity ($D_u = 10$). The frequency of the quantum harmonic trap is chosen as $\omega = 0.08$. The dissipation and pumping rates are $\nu_- = 10^{-4}$ and $\nu_+ = 10^{-8}$, respectively. We set the mass and Planck constant to unity.

Analytical expressions enable a symbolic analysis on the MSD, and mathematical conditions for slopes such as t^6 or t^7 . Also, the reason why t^8 cannot be observed can be found from the following analytical expansion. In the limit of small pumping and dissipation rates, where a t^6 slope was found [22], the expression is given by

$$\langle |\hat{x}(\delta t) - \hat{x}(0)|^2 \rangle \simeq \frac{\omega}{2m} \delta t^2 - \frac{\omega^3}{24m} \delta t^4 + \frac{\omega^5}{720m} \delta t^6 + \frac{D_u \omega^4}{126} \delta t^7 - \frac{\omega^4}{40320 m \tau} (140 D_u m + \tau \omega^3) \delta t^8. \quad (47)$$

The above expression is derived in the small time limit, $\delta t \rightarrow 0$. Eq. (47) implies the existence of t^2 slope, t^6 slope and t^7 slope. Interestingly, a term involving D_u does not appear before the 7-th order term, and a term involving $1/\tau$ does not appear before the 8-th order term. In addition to that, the negative sign of t^8 term indicates that the increasing slope of t^8 in the MSD cannot be found in this limit. As the sign of the t^4 term is also negative, the t^4 slope is absent in this regime. Therefore, a large activity strength suppresses all contributions below seventh order in time and the long persistent time suppresses the eighth order term. This results in t^7 slope in the MSD plot of large D_u and long τ . Conversely, with small D_u reveals t^6 slope as the small intensity suppressed t^7 term. It should be noted that Eq. (47) relies on the small-time approximation and the assumption of weak ν_- and ν_+ , and thus does not capture the full time dependence of the mean squared displacement.

V. THE EFFECT OF THE INITIAL QUANTUM STATE

We have shown that the t^6 and t^7 scalings highly depend on the initial distribution of the state variables of activity (x_c, u) . One may wonder then how the initial quantum state changes the scalings. For this purpose, we consider a squeezed initial quantum state. Squeezed quantum states can have sharp distribution on position or momentum space while conserving the uncertainty relation.

We computed the MSD for various initial conditions by varying the squeezing parameter r and present a comparative plot in Figs. 5 and 6. Explicitly, the squeezed state can be expressed as

$$|\psi_{\text{ini}}\rangle = \hat{S}(r)|0\rangle \quad (48)$$

where $|0\rangle$ is the ground state of the harmonic oscillator at time $t = 0$ and the squeezing operator is given by

$$\hat{S}(r) = \exp\left[\frac{r}{2}(\hat{a}^2 - \hat{a}^{\dagger 2})\right]. \quad (49)$$

Here, r is a real value (for detailed information regarding squeezing operators see section 3.4.3 in Ref. [27]). Squeezing with a positive r results in a position distribution narrowed by a factor of e^{-2r} and a momentum space distribution broadened by a factor e^{2r} . The uncertainty principle thereby continues to hold.

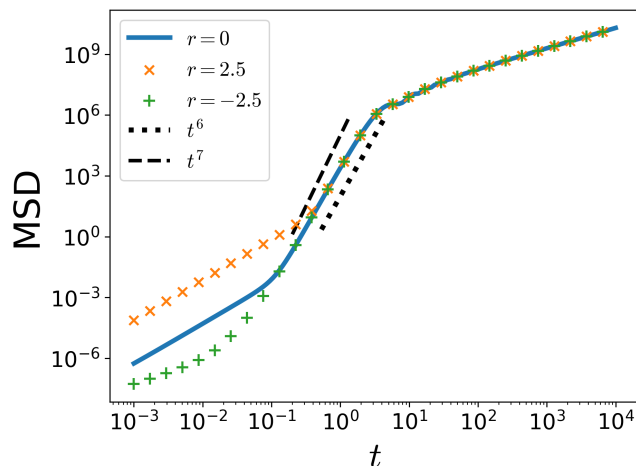


FIG. 5. Plot of MSD [Eq. (36)] versus time of the quantum active particle with three initial conditions. The initial distribution for classical variables are chosen as Eq. (39). The orange ‘ \times ’ marker shows the result of initially squeezed state [Eq. (48)] with $r = 2.5$ and the green ‘ $+$ ’ marker shows the results of initially squeezed state with $r = -2.5$. The solid line represents the unsqueezed case. We set $\omega = 1$, $D_u = 1000$ and $\tau = 1000$. The other parameters are same as that is used for plotting Fig. 4, for which the behavior scales as t^6 .

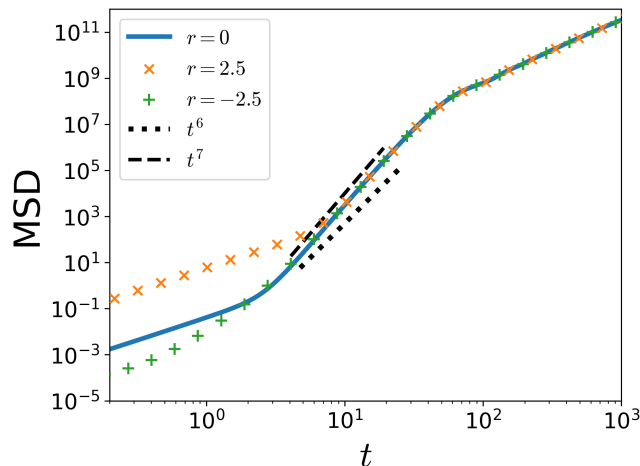


FIG. 6. Plot of MSD [Eq. (36)] versus time of the quantum active particle with three initial conditions. The initial distribution for classical variables are chosen as Eq. (45). The blue line represents the result for an initial ground state of a harmonic trap centered at $x_c = 0$, which is the same result as in Fig. 4 ($D_u = 1000$ and $\tau = 1000$). The orange ‘ \times ’ symbol represent the result with a squeezed initial state [Eq. (48)] of $r = 2.5$. The green ‘ $+$ ’ symbol represents the result with squeezed initial state of $r = -2.5$. The frequency of the quantum harmonic trap is chosen as $\omega = 0.08$. The dissipation and pumping rates are $\nu_- = 10^{-4}$ and $\nu_+ = 10^{-8}$, respectively. The persistent time τ for the activity is 1000, and D_u is also chosen as 1000. We set the mass and Planck constant to unity.

For positive values of r , the initial state exhibits a sharply localized position distribution accompanied by a broadened momentum distribution. Conversely, for negative values of r , the position distribution becomes broadened while the momentum distribution is sharply localized. In all cases, we observe that the t^6 and t^7 scalings of the MSD emerges robustly, indicating that this anomalous scaling behavior is insensitive to the initial quantum state. Also, we find that for $r > 0$ the MSD grows faster than in the unsqueezed case ($r = 0$), whereas for $r < 0$ the growth of the MSD is comparatively slower. This behavior can be attributed to the fact that a broader momentum distribution corresponds to a larger initial kinetic energy, which in turn leads to a more rapid increase of the MSD.

VI. CONCLUSION

In this paper, we revisit the anomalous scaling behavior of the MSD in a system that mimics quantum active matter, and we demonstrated that the hybrid Wigner transformation provides a practical framework for analyzing

quantum active matter that activeness is originated from classical dynamics. Extending previous analyses [22, 23], we evaluate the MSD without relying on the long-time approximation. While the underlying master equation remains valid beyond the small- γ regime as in Ref. [23], our approach enables a systematic analysis of anomalous scaling beyond the small- γ limit considered in Ref. [22]. We also consider initial conditions for which the effects of activity appear already at $t = 0$. In addition, we include the initial conditions used in previous studies [22, 23]

Using a hybrid Wigner master equation, we derive an analytical expression for the MSD and evaluate it numerically. The resulting MSD is independent of sampling and free from statistical fluctuations associated with finite sample sizes. The improved resolution of the MSD, together with the absence of the long-time approximation, allows for a more precise characterization of its scaling behavior. With the initial condition for which the effects of activity appear already at $t = 0$, a clearer t^6 scaling is observed. Furthermore, for the initial conditions employed in earlier works [22, 23], we find that the MSD can exhibit an even steeper scaling regime characterized by t^7 growth in certain parameter regimes, particularly with long persistence time τ of the active noise and in the limit of large diffusion coefficient D_u . In addition, the enhanced resolution enables a clearer resolution of oscillatory behavior in the intermediate-time regime. Under the approximations of small pumping and dissipation rates, we further derive simplified analytical expressions for the MSD that provide insight into the origin of the t^6 and t^7 scaling behaviors. The obtained expressions support the aforementioned conditions under which t^6 and t^7 scaling emerges.

Finally, we examine the robustness of these anomalous scaling regimes with respect to the choice of the initial quantum state. We consider squeezed initial states and demonstrate that the exotic scaling behavior persists. These results highlight the stability of the anomalous scalings and provide a useful framework for analyzing nonequilibrium dynamics in quantum active matter.

ACKNOWLEDGMENTS

M.t.V. is funded by the Deutsche Forschungsgemeinschaft (DFG, German Research Foundation) – SFB 1551, Project-ID 464588647 and by the Carl-Zeiss-Stiftung (Wildcard programme). This study contributes to research done in the Mainz Institute of Multiscale Modeling, M³ODEL.

CODE AVAILABILITY

We provide the Wolfram code [36] used to analytically handle the Wigner transformation, which may facilitate further analytical and numerical studies of quantum active matter.

-
- [1] S. Ramaswamy, The mechanics and statistics of active matter, *Annu. Rev. Condens. Matter Phys.* **1**, 323 (2010).
 - [2] M. C. Marchetti, J.-F. Joanny, S. Ramaswamy, T. B. Liverpool, J. Prost, M. Rao, and R. A. Simha, Hydrodynamics of soft active matter, *Rev. Mod. Phys.* **85**, 1143 (2013).
 - [3] G. Gompper, R. G. Winkler, T. Speck, A. Solon, C. Nardini, F. Peruani, H. Löwen, R. Golestanian, U. B. Kaupp, L. Alvarez, *et al.*, The 2020 motile active matter roadmap, *J. Phys.: Condens. Matter* **32**, 193001 (2020).
 - [4] C. Bechinger, R. Di Leonardo, H. Löwen, C. Reichhardt, G. Volpe, and G. Volpe, Active particles in complex and crowded environments, *Rev. Mod. Phys.* **88**, 045006 (2016).
 - [5] T. Vicsek, A. Czirók, E. Ben-Jacob, I. Cohen, and O. Shochet, Novel type of phase transition in a system of self-driven particles, *Phys. Rev. Lett.* **75**, 1226 (1995).
 - [6] J. Toner and Y. Tu, Long-range order in a two-dimensional dynamical XY model: how birds fly together, *Phys. Rev. Lett.* **75**, 4326 (1995).
 - [7] R. Soto and R. Golestanian, Self-assembly of catalytically active colloidal molecules: tailoring activity through surface chemistry, *Phys. Rev. Lett.* **112**, 068301 (2014).
 - [8] F. Schmidt, B. Liebchen, H. Löwen, and G. Volpe, Light-controlled assembly of active colloidal molecules, *J. Chem. Phys.* **150**, 094905 (2019).
 - [9] A. Cavagna and I. Giardina, Bird flocks as condensed matter, *Annu. Rev. Condens. Matter Phys.* **5**, 183 (2014).
 - [10] S. Ramaswamy, Active matter, *J. Stat. Mech.* **85**, 1143 (2013).
 - [11] P. Baconnier, D. Shohat, C. H. López, C. Coulais, V. Démery, G. Düring, and O. Dauchot, Selective and collective actuation in active solids, *Nat. Phys.* **18**, 1234 (2022).
 - [12] L. Caprini, A. Ldov, R. K. Gupta, H. Ellenberg, R. Wittmann, H. Löwen, and C. Scholz, Emergent memory from tapping collisions in active granular matter, *Commun. Phys.* **7**, 52 (2024).
 - [13] A. P. Antonov, L. Caprini, A. Ldov, C. Scholz, and H. Löwen, Inertial active matter with coulomb friction, *Phys. Rev. Lett.* **133**, 198301 (2024).

- [14] I. S. Aranson, Bacterial active matter, *Rep. Prog. Phys.* **85**, 076601 (2022).
- [15] A. Walther and A. H. Müller, Janus particles, *Soft Matter* **4**, 663 (2008).
- [16] B. Liebchen and H. Lowen, Synthetic chemotaxis and collective behavior in active matter, *Acc. Chem. Res.* **51**, 2982 (2018).
- [17] A.-Y. Jee, Y.-K. Cho, S. Granick, and T. Trusty, Catalytic enzymes are active matter, *Proc. Nat. Acad. Sci.* **115**, E10812 (2018).
- [18] S. Ghosh, A. Somasundar, and A. Sen, Enzymes as active matter, *Annu. Rev. Condens. Matter Phys.* **12**, 177 (2020).
- [19] M. te Vrugt, B. Liebchen, and M. E. Cates, What exactly is 'active matter'?, [arXiv:2507.21621](https://arxiv.org/abs/2507.21621) (2025).
- [20] K. Adachi, K. Takasan, and K. Kawaguchi, Activity-induced phase transition in a quantum many-body system, *Phys. Rev. Res.* **4**, 013194 (2022).
- [21] K. Takasan, K. Adachi, and K. Kawaguchi, Activity-induced ferromagnetism in one-dimensional quantum many-body systems, *Phys. Rev. Res.* **6**, 023096 (2024).
- [22] A. P. Antonov, Y. Zheng, B. Liebchen, and H. Löwen, Engineering active motion in quantum matter, *Phys. Rev. Res.* **7**, 033008 (2025).
- [23] A. P. Antonov, S. Lee, B. Liebchen, H. Löwen, J. Melles, G. Morigi, Y. Tuchkov, and M. te Vrugt, Modeling dissipation in quantum active matter, [arXiv:2511.21502](https://arxiv.org/abs/2511.21502) (2025).
- [24] T. Nadolny, C. Bruder, and M. Brunelli, Nonreciprocal synchronization of active quantum spins, *Phys. Rev. X* **15**, 011010 (2025).
- [25] R. Khasseh, S. Wald, R. Moessner, C. A. Weber, and M. Heyl, Active quantum flocks, *Phys. Rev. Lett.* **135**, 248302 (2023).
- [26] A.-G. Penner, L. Viotti, R. Fazio, L. Arrachea, and F. von Oppen, Heat-to-motion conversion for quantum active matter, *Phys. Rev. B* **112**, L180303 (2025).
- [27] H.-P. Breuer and F. Petruccione, *The theory of open quantum systems* (OUP Oxford, 2007).
- [28] C. Gardiner and P. Zoller, *Quantum noise: a handbook of Markovian and non-Markovian quantum stochastic methods with applications to quantum optics* (Springer Science & Business Media, 2004).
- [29] H. Dekker, Quantization of the linearly damped harmonic oscillator, *Phys. Rev. A* **16**, 2126 (1977).
- [30] S. Lee, M. Ha, J.-M. Park, and H. Jeong, Finite-time quantum otto engine: Surpassing the quasistatic efficiency due to friction, *Phys. Rev. E* **101**, 022127 (2020).
- [31] S. Lee, M. Ha, and H. Jeong, Quantumness and thermodynamic uncertainty relation of the finite-time otto cycle, *Phys. Rev. E* **103**, 022136 (2021).
- [32] I. Yang, T. Agrenius, V. Usova, O. Romero-Isart, and G. Kirchmair, Hot Schrödinger cat states, *Science Advances* **11**, eadr4492 (2025).
- [33] E. Wigner, On the quantum correction for thermodynamic equilibrium, *Phys. Rev.* **40**, 749 (1932).
- [34] H. J. Groenewold, On the principles of elementary quantum mechanics, in *On the principles of elementary quantum mechanics*, Vol. 12 (Springer, 1946) p. 405.
- [35] W. R. Inc., *Mathematica, Version 14.2*, Champaign, IL, 2025.
- [36] Y. Tuchkov and S. Lee, *Symbolic wigner transformation (version 1.0.0)* (2026), <https://doi.org/10.5281/zenodo.19693441>.
- [37] P. Massignan, A. Lampo, J. Wehr, and M. Lewenstein, Quantum brownian motion with inhomogeneous damping and diffusion, *Phys. Rev. A* **91**, 033627 (2015).
- [38] S. Sastry, P. G. Debenedetti, and F. H. Stillinger, Signatures of distinct dynamical regimes in the energy landscape of a glass-forming liquid, *Nature* **393**, 554 (1998).
- [39] T. Albash, S. Boixo, D. A. Lidar, and P. Zanardi, Quantum adiabatic markovian master equations, *New J. Phys.* **14**, 123016 (2012).
- [40] R. Dann, A. Levy, and R. Kosloff, Time-dependent markovian quantum master equation, *Phys. Rev. A* **98**, 052129 (2018).
- [41] N. G. Van Kampen, *Stochastic processes in physics and chemistry*, Vol. 1 (Elsevier, 2007).
- [42] C. Gardiner, *Stochastic methods*, Vol. 4 (Springer Berlin Heidelberg, 1983).
- [43] F. Qirezi, *From Stochastic to Deterministic Langevin Equation*, M.sc. thesis, Queen Mary University of London, London, United Kingdom (2009).
- [44] H. Risken, *The Fokker-Planck Equation* (Springer, 1984) p. 63.

Appendix A: Derivation of Moyal product

Here, we show how the Moyal product appears in Wigner transformation (see Ref. [34]). For completeness and to keep the presentation self-contained, we briefly outline the derivation here. We start from the definition of the Wigner function in terms of position and momentum operators,

$$\begin{aligned}
 W(x, p) &= \frac{1}{\pi\hbar} \int dz e^{-\frac{2ipz}{\hbar}} \langle x + z | \hat{\rho} | x - z \rangle \\
 &= \frac{1}{2\pi\hbar} \int dy e^{-\frac{ipy}{\hbar}} \langle x + \frac{y}{2} | \hat{\rho} | x - \frac{y}{2} \rangle.
 \end{aligned} \tag{A1}$$

Here we define $y = 2z$. To rewrite this expression in a Fourier form, we insert the identity $1 = \int dx' \delta(x' - x + \frac{y}{2})$, which yields

$$\begin{aligned} W(x, p) &= \frac{1}{2\pi\hbar} \int dy \int dx' e^{-\frac{ipy}{\hbar}} \langle x + \frac{y}{2} | \hat{\rho} | x - \frac{y}{2} \rangle \delta\left(x' - x + \frac{y}{2}\right) \\ &= \frac{1}{2\pi\hbar} \int dy \int dx' e^{-\frac{ipy}{\hbar}} \langle x' + y | \hat{\rho} | x' \rangle \delta\left(x' - x + \frac{y}{2}\right). \end{aligned} \quad (\text{A2})$$

Using the relation $\delta(x) = \frac{1}{2\pi\hbar} \int dp_y e^{-\frac{i}{\hbar} p_y x}$, one may obtain

$$W(x, p) = \frac{1}{(2\pi\hbar)^2} \int dy \int dx' \int dp_y e^{-\frac{ipy}{\hbar}} \langle x' + y | \hat{\rho} | x' \rangle e^{-\frac{i}{\hbar} p_y (x' - x + y/2)}. \quad (\text{A3})$$

Using $|x' + y\rangle = e^{-\frac{i}{\hbar} y \hat{p}} |x'\rangle$ and $e^{-\frac{i}{\hbar} p_y x'} |x'\rangle = \langle x' | e^{-\frac{i}{\hbar} p_y \hat{x}}$, the Wigner function becomes

$$W(x, p) = \frac{1}{(2\pi\hbar)^2} \int dy \int dp_y \int dx' e^{\frac{i}{\hbar} (p_y x - p_y y)} \langle x' | e^{-\frac{i}{\hbar} p_y \hat{x}} e^{\frac{i}{\hbar} y \hat{p}} \hat{\rho} | x' \rangle e^{-\frac{i}{\hbar} p_y y/2}. \quad (\text{A4})$$

Using the Baker–Campbell–Hausdorff (BCH) formula,

$$e^{-\frac{i}{\hbar} p_y \hat{x}} e^{\frac{i}{\hbar} y \hat{p}} = e^{-\frac{i}{\hbar} (p_y \hat{x} - y \hat{p})} e^{\frac{i}{2\hbar} p_y y}, \quad (\text{A5})$$

we finally obtain

$$W(x, p) = \frac{1}{(2\pi\hbar)^2} \int dy \int dp_y e^{\frac{i}{\hbar} (p_y x - p_y y)} \text{tr}[e^{-\frac{i}{\hbar} (p_y \hat{x} - y \hat{p})} \hat{\rho}]. \quad (\text{A6})$$

We define the Fourier transform of the Wigner function as

$$\begin{aligned} W_f(y, p_y) &\equiv \iint dx dp W(x, p) e^{-\frac{i}{\hbar} (p_y x - y p)}, \\ &= \text{tr}[e^{-\frac{i}{\hbar} (p_y \hat{x} - y \hat{p})} \hat{\rho}]. \end{aligned} \quad (\text{A7})$$

The density operator can be reconstructed as

$$\hat{\rho} = \iint \frac{dy dp_y}{2\pi\hbar} W_f(y, p_y) e^{\frac{i}{\hbar} (p_y \hat{x} - y \hat{p})}. \quad (\text{A8})$$

Eq. (A8) can be verified as follows: Consider the following trace

$$\text{tr} \left[e^{-\frac{i}{\hbar} (p_y \hat{x} - y \hat{p})} \hat{\rho} \right] = \iint \frac{dp'_y dy'}{2\pi\hbar} W_f(y', p'_y) \text{tr} \left[e^{\frac{i}{\hbar} [(p'_y - p_y) \hat{x} - (y' - y) \hat{p}]} e^{\frac{i}{2\hbar} (y p'_y - p_y y')} \right] \quad (\text{A9})$$

where we replaced $\hat{\rho}$ in the left-hand side with Eq. (A8). Using the BCH formula, we compute the trace

$$\begin{aligned} \text{tr} \left[e^{\frac{i}{\hbar} [(p'_y - p_y) \hat{x} - (y' - y) \hat{p}]} \right] &= \text{tr} \left[e^{\frac{i}{\hbar} (p'_y - p_y) \hat{x}} e^{-\frac{i}{\hbar} (y' - y) \hat{p}} \right] e^{-\frac{i}{2\hbar} (p'_y - p_y)(y' - y)} \\ &= \int dx \langle x | e^{\frac{i}{\hbar} (p'_y - p_y) \hat{x}} e^{-\frac{i}{\hbar} (y' - y) \hat{p}} | x \rangle e^{-\frac{i}{2\hbar} (p'_y - p_y)(y' - y)} \\ &= \int dx e^{\frac{i}{\hbar} (p'_y - p_y) x} \langle x | x + y' - y \rangle e^{-\frac{i}{2\hbar} (p'_y - p_y)(y' - y)} \\ &= \int dx e^{\frac{i}{\hbar} (p'_y - p_y) x} \delta(y' - y) e^{-\frac{i}{2\hbar} (p'_y - p_y)(y' - y)} \\ &= (2\pi\hbar) \delta(p'_y - p_y) \delta(y' - y). \end{aligned} \quad (\text{A10})$$

Substituting Eq. (A10) into Eq. (A9), we obtain

$$\iint \frac{dp'_y dy'}{2\pi\hbar} W_f(y', p'_y) (2\pi\hbar) \delta(p'_y - p_y) \delta(y' - y) e^{\frac{i}{2\hbar} (y p'_y - p_y y')} = \text{tr} \left[e^{-\frac{i}{\hbar} (p_y \hat{x} - y \hat{p})} \hat{\rho} \right]. \quad (\text{A11})$$

The right-hand side is the starting point of this equality, which verifies Eq. (A8).

From the inverse map, we have

$$\hat{\rho} = \iint \frac{dy dp_y}{2\pi\hbar} W_f(y, p_y) e^{\frac{i}{\hbar}(p_y \hat{x} - y \hat{p})} = \iint \frac{dy dp_y}{2\pi\hbar} \text{tr} \left[e^{-\frac{i}{\hbar}(p_y \hat{x} - y \hat{p})} \hat{\rho} \right] e^{\frac{i}{\hbar}(p_y \hat{x} - y \hat{p})}. \quad (\text{A12})$$

This implies the identity super operator

$$\mathcal{I}[\cdot] = \iint \frac{dy dp_y}{2\pi\hbar} \text{tr} \left[e^{-\frac{i}{\hbar}(p_y \hat{x} - y \hat{p})} \cdot \right] e^{\frac{i}{\hbar}(p_y \hat{x} - y \hat{p})}. \quad (\text{A13})$$

We now have all the ingredients to establish the relation between the Moyal product and the Wigner transformation. We define χ as

$$\chi[\hat{A}](y, p_y) \equiv \text{tr} \left\{ e^{-\frac{i}{\hbar}(p_y \hat{x} - y \hat{p})} \hat{A} \right\}, \quad (\text{A14})$$

which is related to the Wigner function by

$$W(x, p) = W[\hat{\rho}](x, p) = \frac{1}{(2\pi\hbar)^2} \iint dy dp_y e^{\frac{i}{\hbar}(p_y x - y p)} \chi[\hat{\rho}](y, p_y) \quad (\text{A15})$$

and the Wigner transformation of an operator by

$$W[\hat{A}](x, y) = \frac{1}{2\pi\hbar} \iint dy dp_y e^{\frac{i}{\hbar}(p_y x - y p)} \chi[\hat{A}](y, p_y). \quad (\text{A16})$$

Using the completeness of the Weyl operator basis, an operator can be expanded as

$$\hat{A} = \iint \frac{dy dp_y}{2\pi\hbar} \chi[\hat{A}](y, p_y) e^{\frac{i}{\hbar}(p_y \hat{x} - y \hat{p})}. \quad (\text{A17})$$

Therefore, the product $\hat{A}\hat{B}$ can be written as

$$\begin{aligned} \hat{A}\hat{B} &= \iint \frac{dp_y dy}{2\pi\hbar} \chi[\hat{A}](y, p_y) e^{\frac{i}{\hbar}(p_y \hat{x} - y \hat{p})} \iint \frac{dp'_y dy'}{2\pi\hbar} \chi[\hat{B}](y', p'_y) e^{\frac{i}{\hbar}(p'_y \hat{x} - y' \hat{p})} \\ &= \iiint \frac{dp_y dy}{2\pi\hbar} \frac{dp'_y dy'}{2\pi\hbar} \chi[\hat{A}](y, p_y) \chi[\hat{B}](y', p'_y) e^{\frac{i}{\hbar}[(p_y + p'_y)\hat{x} - (y + y')\hat{p}]} e^{\frac{i}{2\hbar}(p_y y' - y p'_y)}, \end{aligned} \quad (\text{A18})$$

where we used the BCH identity (A5) in the form

$$e^{\frac{i}{\hbar}(\xi \hat{p} - \eta \hat{x})} e^{\frac{i}{\hbar}(\xi' \hat{p} - \eta' \hat{x})} = e^{\frac{i}{\hbar}[(\xi + \xi')\hat{p} - (\eta + \eta')\hat{x}]} e^{\frac{i}{\hbar}(\eta \xi' - \xi \eta')}. \quad (\text{A19})$$

One may obtain

$$\begin{aligned} W[\hat{A}\hat{B}](x, p) &= \iiint \frac{dp_y dy}{2\pi\hbar} \frac{dp'_y dy'}{2\pi\hbar} \chi[\hat{A}](p_y, y) \chi[\hat{B}](p'_y, y') \\ &\quad \times e^{\frac{i}{\hbar}[(p_y + p'_y)x - (y + y')p]} e^{\frac{i}{2\hbar}(p_y y' - y p'_y)} \end{aligned} \quad (\text{A20})$$

after applying the Wigner transformation for an operator to both sides of Eq. (A18), because

$$\begin{aligned} W \left[e^{\frac{i}{\hbar}[(p_y + p'_y)\hat{x} - (y + y')\hat{p}]} \right] (x, p) &= \frac{1}{2\pi\hbar} \iint d\tilde{p}_y d\tilde{y} e^{\frac{i}{\hbar}(\tilde{p}_y x - \tilde{y} p)} \text{tr} \left[e^{-\frac{i}{\hbar}(\tilde{p}_y \hat{x} - \tilde{y} \hat{p})} e^{\frac{i}{\hbar}[(p_y + p'_y)\hat{x} - (y + y')\hat{p}]} \right] \\ &= \frac{1}{2\pi\hbar} \iint d\tilde{p}_y d\tilde{y} e^{\frac{i}{\hbar}(\tilde{p}_y x - \tilde{y} p)} \text{tr} \left[e^{\frac{i}{2\hbar}[-\tilde{y}(-p_y - p'_y) - \tilde{p}_y(y + y')]} e^{\frac{i}{\hbar}[(p_y + p'_y - \tilde{p}_y)\hat{x} - (y + y' - \tilde{y})\hat{p}]} \right] \\ &= \frac{1}{2\pi\hbar} \iint d\tilde{p}_y d\tilde{y} e^{\frac{i}{\hbar}(\tilde{p}_y x - \tilde{y} p)} (2\pi\hbar) \delta(y + y' - \tilde{y}) \delta(p_y + p'_y - \tilde{p}_y) \\ &= \exp \left[\frac{i}{\hbar}((p_y + p'_y)x - p(y + y')) \right]. \end{aligned} \quad (\text{A21})$$

Expanding the phase factor in powers of $(\eta\xi' - \xi\eta')$, we get

$$W[\hat{A}\hat{B}](x, p) = \sum_{n=0}^{\infty} \frac{1}{n!} \left(\frac{i}{2\hbar}\right)^n \iiint \frac{dp_y dy dp'_y dy'}{2\pi\hbar} \chi[\hat{A}](p_y, y) e^{\frac{i}{\hbar}(p_y x - yp)} \chi[\hat{B}](p'_y, y') e^{\frac{i}{\hbar}(p'_y x - y' p)} \times (p_y y' - y p'_y)^n. \quad (\text{A22})$$

Using the identities

$$p_y e^{\frac{i}{\hbar}(p_y x - yp)} = \frac{\hbar}{i} \partial_x e^{\frac{i}{\hbar}(p_y x - yp)}, \quad y e^{\frac{i}{\hbar}(p_y x - yp)} = -\frac{\hbar}{i} \partial_p e^{\frac{i}{\hbar}(p_y x - yp)} \quad (\text{A23})$$

and the definition of Wigner transformation of observable, the above expression can be rewritten as

$$W[\hat{A}\hat{B}](x, p) = \sum_{n=0}^{\infty} \frac{1}{n!} W[\hat{A}](x, p) \left[\frac{i\hbar}{2} \left(\overleftarrow{\partial}_x \overrightarrow{\partial}_p - \overleftarrow{\partial}_p \overrightarrow{\partial}_x \right) \right]^n W[\hat{B}](x, p). \quad (\text{A24})$$

Finally, we obtain the Moyal product formula

$$W[\hat{A}\hat{B}](x, p) = W[\hat{A}](x, p) \exp \left[\frac{i\hbar}{2} \left(\overleftarrow{\partial}_x \overrightarrow{\partial}_p - \overleftarrow{\partial}_p \overrightarrow{\partial}_x \right) \right] W[\hat{B}](x, p) \equiv W[\hat{A}] \star W[\hat{B}], \quad (\text{A25})$$

where \star denotes the Moyal product.

Appendix B: Equivalence between Wigner and operator expectation value

Consider the phase-space integral

$$\begin{aligned} \int dx dp A(x, p) W(x, p) &= \frac{2}{\pi\hbar} \int dx dp dz dz' e^{-\frac{2ip}{\hbar}(z+z')} \langle x+z | \hat{A} | x-z \rangle \langle x+z' | \hat{\rho} | x-z' \rangle \\ &= 2 \int dx dz dz' \delta(z+z') \langle x+z | \hat{A} | x-z \rangle \langle x-z | \hat{\rho} | x+z \rangle \\ &= 2 \int dx dz \langle x+z | \hat{A} | x-z \rangle \langle x-z | \hat{\rho} | x+z \rangle. \end{aligned} \quad (\text{B1})$$

Here, performing the p integration yields a delta function.

By introducing new variables $s = x+z$ and $s' = x-z$, the integral becomes

$$\begin{aligned} \int dx dp A(x, p) W(x, p) &= \int ds ds' \langle s | \hat{A} | s' \rangle \langle s' | \hat{\rho} | s \rangle \\ &= \text{tr} \{ \hat{A} \hat{\rho} \}. \end{aligned} \quad (\text{B2})$$

Therefore, the average in the Wigner representation is same as the average with the corresponding quantum operator and the density matrix.

In the case of a two-time function, two expectations,

$$\text{tr} \{ \hat{A}(t) \hat{B}(0) \hat{\rho} \} \quad (\text{B3})$$

and

$$\int dx dp W[\hat{A}(t)](x, p) W[\hat{B}(0)](x, p) W(x, p), \quad (\text{B4})$$

are not equivalent in general. Here, $W[\hat{A}]$ is defined in Eq. (A16). However, if $\hat{A}(t)$ and $\hat{B}(0)$ are linear to \hat{x} and \hat{p} , then the two expectations

$$\frac{1}{2} \text{tr} \{ \hat{A}(t) \hat{B}(0) \hat{\rho} + \hat{B}(0) \hat{A}(t) \hat{\rho} \} \text{ and } \int dx dp W[A(t)](x, p) W[B(0)](x, p) W(x, p) \quad (\text{B5})$$

are equivalent. In Appendix. E, we explain the conditions when the evolution of moments is closed under the Lindblad master equation and can be a linear combination of basis operators. proof starts from Eq. (B2):

$$\text{tr} \left\{ (\hat{A}(t)\hat{B}(0) + \hat{B}(0)\hat{A}(t))\hat{\rho} \right\} = \iint dx dp W[(\hat{A}(t)\hat{B}(0) + \hat{B}(0)\hat{A}(t))]W(x, p, 0) \quad (\text{B6})$$

The Wigner transformation of the symmetric operator is given by

$$W \left[\hat{A}(t)\hat{B}(0) + \hat{B}(0)\hat{A}(t) \right] = W[\hat{A}(t)] \star W[\hat{B}(0)] + W[\hat{B}(0)] \star W[\hat{A}(t)] \quad (\text{B7})$$

When \hat{A} and \hat{B} are linear combinations of \hat{x} and \hat{p} , the above equality can be rearranged as

$$\begin{aligned} W \left[\hat{A}(t)\hat{B}(0) + \hat{B}(0)\hat{A}(t) \right] &= 2 W[\hat{A}(t)] W[\hat{B}(0)] \\ &\quad + \frac{i}{2} W[\hat{A}(t)] \left(\overleftarrow{\partial}_x \overrightarrow{\partial}_p - \overleftarrow{\partial}_p \overrightarrow{\partial}_x \right) W[\hat{B}(0)] \\ &\quad - \frac{i}{2} W[\hat{B}(0)] \left(\overleftarrow{\partial}_x \overrightarrow{\partial}_p - \overleftarrow{\partial}_x \overrightarrow{\partial}_q \right) W[\hat{A}(t)] \\ &= 2W[\hat{A}(t)] W[\hat{B}(0)]. \end{aligned} \quad (\text{B8})$$

Therefore, the symmetrized two-time correlation function and the corresponding two-time correlation function in the Wigner representation are equivalent:

$$\begin{aligned} \frac{1}{2} \left(\text{tr} \{ \hat{A}(t)\hat{B}(0)\hat{\rho}(0) \} + \text{tr} \{ \hat{B}(0)\hat{A}(t)\hat{\rho}(0) \} \right) &= \int dx dp W[\hat{A}(t)] W[\hat{B}(0)] W(x, p, 0) \\ &= \int dx dp A_W(t) B_W(0) W(x, p, 0). \end{aligned} \quad (\text{B9})$$

Appendix C: Wolfram note

We utilize a *Mathematica* file to transform a given quantum master equation [36] to the Wigner representation. The shared code is based on *Wolfram Mathematica* version 14.2.0. In order to symbolically compute the Wigner transform as in (5), the symbolic algebra programming language *Mathematica* was employed. The code implements the Moyal (star) product of two quantum operators by realizing it as a truncated exponential of a bidifferential operator (A25) acting on phase-space symbols, namely the Wigner transforms of the corresponding observables. In deformation quantization, operators depending on the canonical position and momentum operators \hat{q} and \hat{p} are represented by functions $f(q, p)$ and $g(q, p)$ on phase space, and their operator product is mapped to the Moyal product

$$(f \star g)(q, p) = f(q, p) \exp \left[\frac{i\hbar}{2} \left(\overleftarrow{\partial}_q \overrightarrow{\partial}_p - \overleftarrow{\partial}_p \overrightarrow{\partial}_q \right) \right] g(q, p), \quad (\text{C1})$$

where the arrows indicate whether the derivatives act on f or on g .

Thus, the symbols f and g are treated as symbolic functions of q and p within the *Mathematica* environment. It is important to note that, in our case, the symbolic functions f and g are always finite-degree polynomials in q and p . Indeed, the dissipator of interest (22) is composed of products of the operators $a(t)$ and $a^\dagger(t)$ (23), which themselves are linear symbolic functions of q and p .

The routine `poissonOp` encodes the generator of this exponential, namely the Poisson-type bidifferential operator

$$\mathcal{P} = \frac{i\hbar}{2} (\partial_{q_1} \partial_p - \partial_{p_1} \partial_q), \quad (\text{C2})$$

where auxiliary variables (q_1, p_1) are introduced to disentangle the left- and right-acting derivatives on $f(q_1, p_1)$ and $g(q, p)$, respectively. The Poisson operator \mathcal{P} thus acts on the function $(q_1, p_1, q, p) \mapsto f(q_1, p_1)g(q, p)$. Its implementation reads

```
poissonOp[q1_, p1_, q_, p_] :=
  Function[fg, (I \[HBar])/2 (D[fg, q1, p] - D[fg, p1, q])];
```

The function `operatorExp` constructs the exponential $\exp(\mathcal{P})$ by iteratively applying \mathcal{P} and summing the resulting series up to a fixed order n ,

$$\exp(\mathcal{P})h = \sum_{k=0}^n \frac{1}{k!} \mathcal{P}^k h + \mathcal{O}(\hbar^{n+1}), \quad (\text{C3})$$

which corresponds to truncating the formal power-series expansion of the exponential in powers of \hbar and h is the test function on which the operator $\exp(\mathcal{P})$ acts. This truncation becomes exact for $n \geq 3$, since the dissipator is a polynomial in q and p of degree three, while the Hamiltonian (18) is of degree two.

The `operatorExp` function relies on the recurrence relation and for $n \geq 0$

$$t_{n+1} = \frac{\mathcal{P}(t_n)}{n+1}, \quad S_{n+1} = S_n + t_{n+1} \quad (\text{C4})$$

with initial values $S_1 = h$ and $T_1 = h$, to construct successive partial sums S_k of the exponential series. Here S_n is the partial sum of (C3) and t_n is the n -th term in that sum. The computation is terminated either after n iterations or earlier if $S_{k+1} = S_k$, which typically occurs due to vanishing higher-order derivatives for polynomial symbols. This logic is implemented using `FixedPoint` as

```
operatorExp[dop_, n_ : NMAX][A_] :=
  First@FixedPoint[{-#[[1]] + dop[#[[2]]],
    dop[#[[2]]]/#[[3]], #[[3]] + 1} &, {A, A, 2}, n,
    SameTest -> (PossibleZeroQ[#[[1]] - #2[[1]]] &);
```

In `MoyalProd`, the first symbol is rewritten as $f(q_1, p_1)$ and multiplied with $g(q, p)$, after which the truncated exponential $\exp(\mathcal{P})$ acts on the product. Identifying the auxiliary and physical variables, $q_1 \rightarrow q$ and $p_1 \rightarrow p$, yields the Moyal product

$$f \star g = \exp(\mathcal{P})(f(q_1, p_1)g(q, p))\Big|_{q_1=q, p_1=p}. \quad (\text{C5})$$

The corresponding implementation is

```
MoyalProd[f_, g_, q_ : q, p_ : p, n_ : NMAX] :=
  Module[{q1, p1},
    operatorExp[poissonOp[q1, p1, q, p], n]
    [(f /. {q -> q1, p -> p1})*g] /. {q1 -> q, p1 -> p};
```

Finally, the `MoyalBracket` is defined as the antisymmetrized star product divided by $i\hbar$,

$$\{f, g\}_M = \frac{1}{i\hbar}(f \star g - g \star f), \quad (\text{C6})$$

with the implementation

```
MoyalBracket[f_, g_, q_ : q, p_ : p, n_ : NMAX] :=
  (MoyalProd[f, g, q, p, n] - MoyalProd[g, f, q, p, n])/(I \[HBar]);
```

Appendix D: Calculation of the two-time correlation function using a quasi-classical Langevin equation

The Cartesian product for $\mathbf{q}(t_1)$ and $\mathbf{q}(t_2)$ is given by

$$\begin{aligned} \mathbf{q}(t_1) \otimes \mathbf{q}(t_2) &= [e^{-At_1} \mathbf{q}(0) + \int_0^{t_1} ds_1 e^{-A(t_1-s_1)} B \boldsymbol{\eta}(s_1)] \otimes [e^{-At_2} \mathbf{q}(0) + \int_0^{t_2} ds_2 e^{-A(t_2-s_2)} B \boldsymbol{\eta}(s_2)]^T \\ &= e^{-At_1} \mathbf{q}(0) \otimes \mathbf{q}(0) e^{-A^T t_2} + \int_0^{t_1} ds_1 \int_0^{t_2} ds_2 e^{-A(t_1-s_1)} B \boldsymbol{\eta}(s_1) \otimes \boldsymbol{\eta}(s_2) B^T e^{-A^T(t_2-s_2)}. \end{aligned} \quad (\text{D1})$$

After averaging over trajectories,

$$\langle \mathbf{q}(t_1) \otimes \mathbf{q}(t_2) \rangle = e^{-At_1} \langle \mathbf{q}(0) \otimes \mathbf{q}(0) \rangle e^{-A^T t_2} + \int_0^{\min(t_1, t_2)} ds_1 \int_0^{\min(t_1, t_2)} ds_2 e^{-A(t_1-s_1)} B \langle \boldsymbol{\eta}(s_1) \otimes \boldsymbol{\eta}(s_2) \rangle B^T e^{-A^T(t_2-s_2)}. \quad (\text{D2})$$

The stochastic differential equation [Eq. (33)] has the linear drift term, which is named Ornstein-Uhlenbeck process. In this case, the vector \mathbf{q} can be written as

$$\mathbf{q}(t) = e^{-At}\mathbf{q}(0) + \int_0^t ds e^{-A(t-s)}B\boldsymbol{\eta}(s), \quad (\text{D3})$$

and the matrix for the 2nd moment is given by

$$\langle \mathbf{q}(t) \otimes \mathbf{q}(t) \rangle = e^{-At} \langle \mathbf{q}(0) \otimes \mathbf{q}(0) \rangle e^{-A^T t} + 2 \int_0^t ds e^{-A(t-s)} BB^T e^{-A^T(t-s)}. \quad (\text{D4})$$

For $t_1 = t$ and $t_2 = 0$, the two-time correlation function becomes

$$\langle \mathbf{q}(t) \otimes \mathbf{q}(0) \rangle = e^{-At} \langle \mathbf{q}(0) \otimes \mathbf{q}(0) \rangle. \quad (\text{D5})$$

Appendix E: Heisenberg picture

In the Heisenberg picture, the equation of motion for an operator \hat{O} is given by

$$\frac{d\hat{O}}{dt} = \frac{i}{\hbar} [\hat{H}, \hat{O}] + \sum_k \left(\hat{L}_k^\dagger \hat{O} \hat{L}_k - \frac{1}{2} \{ \hat{L}_k^\dagger \hat{L}_k, \hat{O} \} \right). \quad (\text{E1})$$

The commutator is

$$[\hat{L}_k^\dagger \hat{L}_k, \hat{O}] = \hat{L}_k^\dagger [\hat{L}_k, \hat{O}] + [\hat{L}_k^\dagger, \hat{O}] \hat{L}_k. \quad (\text{E2})$$

The dissipator term can be written as

$$\left(\hat{L}_k^\dagger \hat{O} \hat{L}_k - \frac{1}{2} \{ \hat{L}_k^\dagger \hat{L}_k, \hat{O} \} \right) = \hat{L}_k^\dagger [\hat{O}, \hat{L}_k] - \frac{1}{2} \hat{L}_k^\dagger [\hat{O}, \hat{L}_k] - \frac{1}{2} [\hat{O}, \hat{L}_k] \hat{L}_k. \quad (\text{E3})$$

If the commutator $[\hat{O}, \hat{L}_k]$ is a c -number, the dissipative term does not generate higher-order operator products. More generally, if the action of the Lindbladian on a given operator set $\{\hat{O}_\alpha\}$ is closed within its linear span, the Heisenberg equations of motion constitute a closed set of coupled equations.

$$\hat{O}(t) = \sum_\alpha c_\alpha(t) \hat{O}_\alpha + c_0(t) \mathbb{I}, \quad (\text{E4})$$

where the coefficients $c_\alpha(t)$ are time-dependent scalar functions. Consequently, the Heisenberg dynamics reduces to a finite-dimensional linear problem for these coefficients, and no additional operators are generated during the time evolution.

Appendix F: the difference between two moments

In the main text, we employ one definition of the mean-square displacement, whereas Ref. [21] uses another definition for the quantum MSD. Here, we examine whether the t^7 scaling persists under this alternative definition. The definition adopted in Ref. [22] is given as follows

$$(\text{alternative MSD}) = \langle \hat{x}(t)^2 \rangle - \langle \hat{x}(0)^2 \rangle, \quad (\text{F1})$$

which approximates $\langle \hat{x}(t)\hat{x}(0) \rangle + \langle \hat{x}(0)\hat{x}(t) \rangle \sim \langle \hat{x}^2(0) \rangle$

In Fig. 7, we plot the quantum MSD based on the alternative definition using the same set of parameters as in the main text. We find that the t^7 slope remains under identical parameter conditions, showing that the t^7 scaling is robust with respect to the choice of MSD definition.

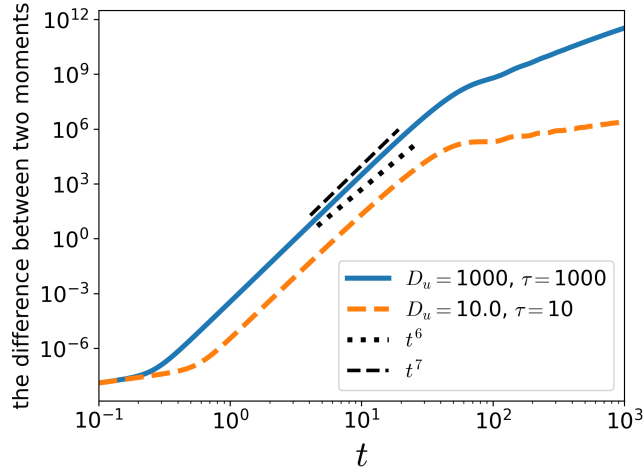


FIG. 7. Plot of the difference between two moments, $\langle \hat{x}^2(t) \rangle_{x_c} - \langle \hat{x}^2(0) \rangle_{x_c}$, versus time of the quantum active particle. The blue solid line represents the case of long persistent time ($\tau = 1000$) and high intensity ($D_u = 1000$). The orange solid line represents the case of shorter persistent time ($\tau = 10$) and lower intensity ($D_u = 10$). The frequency of the quantum harmonic trap is chosen as $\omega = 0.08$. The dissipation and pumping rates are $\nu_- = 10^{-4}$ and $\nu_+ = 10^{-8}$, respectively. We set the mass and Planck constant to unity.

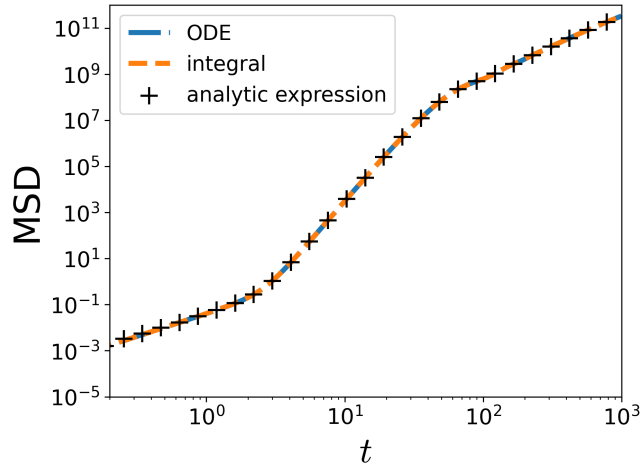


FIG. 8. Plot of MSD versus time of the quantum active particle calculated with three different methods. The blue line represents the result obtained by solving Eq. (G1). The orange line represents the result obtained by numerically evaluating integral expression, Eq. (36). The cross symbol represents the analytically evaluated MSD; the explicit expression of MSD is omitted due to its complexity. The parameters all the same in Fig. 4 with $D_u = 1000$ and $\tau = 1000$.

Appendix G: Evaluating the two-time function

An alternative way to evaluate the two-time function in Eq. (36) is to solve the differential equation

$$\partial_t \langle \mathbf{q}(t) \otimes \mathbf{q}(t) \rangle = -A \langle \mathbf{q}(t) \otimes \mathbf{q}(t) \rangle - \langle \mathbf{q}(t) \otimes \mathbf{q}(t) \rangle A^T + 2BB^T \quad (\text{G1})$$

instead of directly evaluating the integrals in Eq. (36). We solved the above differential equation for plots in this paper. Another method is to numerically evaluate the analytical expression. In Fig. 8, we show that three methods agree within the given parameters. In the case of analytical expression, its precision is low due to many exponential expressions, particularly when $t \gg 10^3$.

Appendix H: Hybrid Wigner master equation

For a given classical trajectory $\Gamma_c = \{x_c(t)\}$, the evolution of the conditional density matrix $\hat{\rho}_c$ is governed by

$$\frac{d}{dt}\hat{\rho}_c(t) = -\frac{i}{\hbar}[\hat{H}(x_c(t)), \hat{\rho}_c(t)] + \mathcal{D}_{x_c}\hat{\rho}_c(t). \quad (\text{H1})$$

Applying the Wigner transform, one may derive

$$\partial_t W(x, p, t|\Gamma_c) = \mathcal{L}_W W(x, p, t|\Gamma_c), \quad (\text{H2})$$

where $\Gamma_c = \{x_c(t), u_c(t)\}$ and \mathcal{L}_W depends on current state $x_c(t)$ at time t . Then, we define a hybrid quasi-probability distribution which combines x_c trajectory probability $P(\Gamma_c)$ and the conditional Wigner function $W(x, p, t|\Gamma_c)$

$$W(x, p, x_c, u, t) \equiv \int \mathcal{D}[\Gamma_c] W(x, p, t|\Gamma_c) P[\Gamma_c] \delta(x_c - x_c(t)) \delta(u - u_c(t)). \quad (\text{H3})$$

We call this function a hybrid quasi-probability distribution. After taking the time derivative of this object, one may derive

$$\begin{aligned} \partial_t W(x, p, x_c, u, t) &= \int \mathcal{D}[\Gamma_c] \partial_t W(x, p, t|\Gamma_c) P[\Gamma_c] \delta(x_c - x_c(t)) \delta(u - u_c(t)) \\ &\quad + \int \mathcal{D}[\Gamma_c] W(x, p, t|\Gamma_c) P[\Gamma_c] \partial_t [\delta(x_c - x_c(t)) \delta(u - u_c(t))]. \end{aligned} \quad (\text{H4})$$

Using Eq. (H2), the first term on the right hand side of Eq. (H4) can be expressed in terms of the operator \mathcal{L}_W . Since \mathcal{L}_W depends on x_c only at time t , the first term can be written as

$$\begin{aligned} \int \mathcal{D}[\Gamma_c] \partial_t W(x, p, t|\Gamma_c) \delta(x_c - x_c(t)) \delta(u - u_c(t)) &= \int \mathcal{D}[\Gamma_c] \mathcal{L}_W W(x, p, t|\Gamma_c) P[\Gamma_c] \delta(x_c - x_c(t)) \delta(u - u_c(t)) \\ &= \mathcal{L}_W W(x, p, x_c, u, t). \end{aligned} \quad (\text{H5})$$

The second term of Eq. (H4) can be expressed with two terms as

$$\int \mathcal{D}[\Gamma_c] W(x, p, t|\Gamma_c) P[\Gamma_c] \partial_t [\delta(x_c - x_c(t))] \delta(u - u_c(t)) \quad (\text{H6})$$

and

$$\int \mathcal{D}[\Gamma_c] W(x, p, t|\Gamma_c) P[\Gamma_c] \delta(x_c - x_c(t)) \partial_t [\delta(u - u_c(t))]. \quad (\text{H7})$$

For each term, we follow a procedure similar to the Kramer-Moyal expansion [41]. To this end, we introduce a test function ϕ and consider the following expression:

$$\begin{aligned} &\int dx_c \phi(x_c) \int \mathcal{D}[x_c(t)] W(x, p, t|\Gamma_c) P[\Gamma_c] \partial_t [\delta(x_c - x_c(t))] \delta(u - u_c(t)) \\ &= \sum_{n=1}^{\infty} \frac{1}{n!} \int dx_c \phi(x_c) (-\partial_{x_c})^n \int \mathcal{D}[\Gamma_c] M_{n, x_c(t)} W(x, p, t|\Gamma_c) P[\Gamma_c] \delta(x_c - x_c(t)) \delta(u - u_c(t)) \\ &= \sum_{n=1}^{\infty} \frac{1}{n!} \int dx_c [\partial_{x_c}^n \phi(x_c)] M_{n, x_c} \int \mathcal{D}[\Gamma_c] W(x, p, t|\Gamma_c) P[\Gamma_c] \delta(x_c - x_c(t)) \delta(u - u_c(t)) \\ &= \sum_{n=1}^{\infty} \frac{1}{n!} \int d\Gamma_c \phi(x_c) (-\partial_{x_c})^n M_{n, x_c} W(x, p, x_c, u, t). \end{aligned} \quad (\text{H8})$$

Here, $M_{n, x_c(t)} = \lim_{\delta t \rightarrow 0} [\delta x_c(t)]^n \delta t^{-1}$, which may be calculated using the Ito calculus and subsequently expressed in terms of $x_c(t)$. Because the M_{n, x_c} term in Eq. (H8) is a function of x_c , the term is independent of the integration variable Γ_c of the path integral $\int \mathcal{D}[\Gamma_c]$. After applying the same procedure to Eq. (H7), the summation of Eq. (H6) and Eq. (H7) is rearranged by $\mathcal{L}_{FP} W(x, p, x_c, u, t)$. Finally, the following master equation is derived

$$\partial_t W(x, p, x_c, u, t) = \mathcal{L}_W W(x, p, x_c, u, t) + \mathcal{L}_{FP} W(x, p, x_c, u, t). \quad (\text{H9})$$

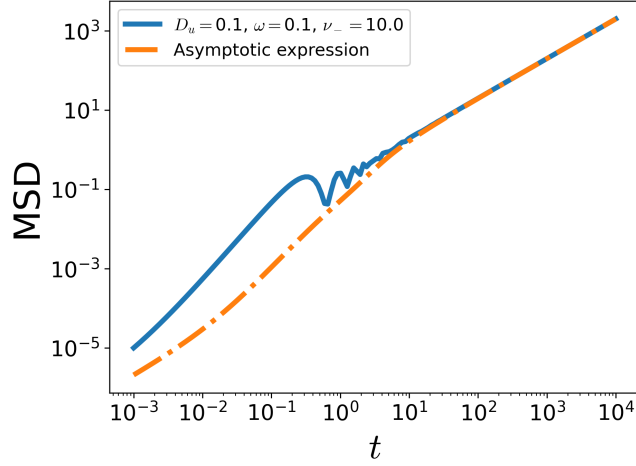


FIG. 9. Plot of MSD versus time of the quantum active particle. $\tau = 1$. The dash-dot line represents the asymptotic expression (Eq. (II)). The hierarchy between the three characteristic times is set to be $\tau \gg 1/\omega, 1/\gamma$.

Appendix I: Asymptotic form in the long time limit

In the long time limit, the MSD of the quantum active matter system discussed in the main text [Eq. (17)] can be written as

$$\langle |\hat{x}(t) - \hat{x}(0)|^2 \rangle \sim 2D_u\tau^2 t + B_0 \left[-g_2(t)e^{-2t/\tau} + g_1(t)e^{-t/\tau} - g_0 \right]. \quad (\text{I1})$$

where

$$B_0 = \frac{D_u}{32(1 + \tau^2\omega^2)^2}, \quad (\text{I2})$$

$$g_0 = 16\tau^5\omega^2(4 + \tau(4 + \tau(4 + 3\tau)\omega^2)), \quad (\text{I3})$$

$$g_1(t) = 16\tau^5\omega^2(1 + t + \tau)(4 + 4\tau^2\omega^2), \quad (\text{I4})$$

and

$$g_2(t) = 16\tau^7\omega^4(2t + \tau). \quad (\text{I5})$$

The assumptions for the derivation are neglecting three terms that involves the initial condition in Eq. (36). Since the initial condition information will be dissappeared in the long time limit. Also, we consider the hierarchy among characteristic times as $\tau \gg 1/\omega, 1/\gamma$. Under these assumptions, the MSD tensor can be rearranged by

$$\langle (\mathbf{q}(t) - \mathbf{q}(0)) \otimes (\mathbf{q}(t) - \mathbf{q}(0)) \rangle \sim 2 \int_0^t e^{-A(t-s)} BB^T e^{-A^T(t-s)} ds. \quad (\text{I6})$$

$e^{-A(t-s)}$ term has four modes as the matrix A has four eigenvalues λ_i and their left and right eigenvectors $|R_i\rangle$ and $\langle L_i|$. Here $\langle L_i|R_j\rangle = \delta_{ij}$. The eigenvalues are $\lambda_1 = 0$, $\lambda_2 = 1/\tau$, $\lambda_3 = \gamma/4 - i\omega$ and $\lambda_4 = \gamma/4 + i\omega$. Because γ is a large value, the eigen modes of λ_3 and λ_4 will be fast decayed in the long time limit. So, we neglect eigen modes of λ_3 and λ_4 .

$$\langle (\mathbf{q}(t) - \mathbf{q}(0)) \otimes (\mathbf{q}(t) - \mathbf{q}(0)) \rangle \sim 2 \int_0^t (|R_1\rangle\langle L_1| + |R_2\rangle\langle L_2| e^{-\lambda_2(t-s)}) BB^T (|L_1\rangle\langle R_1| + |L_2\rangle\langle R_2| e^{-\lambda_2(t-s)}). \quad (\text{I7})$$

After rearranging the (0,0) component of $\langle (\mathbf{q}(t) - \mathbf{q}(0)) \otimes (\mathbf{q}(t) - \mathbf{q}(0)) \rangle$, the asymptotic expression, Eq. (II) can be derived. In Fig. 9, we plot Eq. (II). In the long-time limit it shows good agreement.

Appendix J: Derivation of Eq. (46)

With the initial condition $u(0) = 0$ and $x_c(0) = 0$, the mean squared distance of x_c is different [44]. To derive it, we start from

$$\dot{x}_c(t) = e^{-t/\tau}u(0) + \int_0^t ds_2 e^{-\frac{1}{\tau}(t-s_2)}\sqrt{D}\eta_u(s_2), \quad (\text{J1})$$

where $\langle \eta(t)\eta(t') \rangle = 2\delta(t-t')$. Since $u(0) = 0$, x_c at time t is written by

$$x_c(t) = \int_0^t ds_1 \int_0^{s_1} ds_2 e^{-\frac{1}{\tau}(t-s_2)}\sqrt{D}\eta_u(s_2). \quad (\text{J2})$$

Then, the MSD of x_c is given by

$$\begin{aligned} \langle |x_c(t) - x_c(0)|^2 \rangle &= \int_0^t ds'_1 \int_0^t ds'_2 e^{-(s'_1+s'_2)/\tau} \int_0^{s'_1} ds_1 \int_0^{s'_2} ds_2 D e^{(s_1+s_2)/\tau} \langle \eta_u(s_1)\eta_u(s_2) \rangle \\ &= \int_0^t ds'_1 \int_0^t ds'_2 e^{-(s'_1+s'_2)/\tau} \int_0^{s'_1} ds_1 \int_0^{s'_2} ds_2 D e^{(s_1+s_2)/\tau} \delta(s_1 - s_2) \\ &= D_u \tau^2 [(-3 - e^{-2t/\tau} + 4e^{-t/\tau})\tau + 2t]. \end{aligned} \quad (\text{J3})$$